

6-2009

UWB Antennas for Medical Imaging

Khabat Ebnabbasi
University of Texas-Pan American

Follow this and additional works at: https://scholarworks.utrgv.edu/leg_etd



Part of the [Electrical and Computer Engineering Commons](#)

Recommended Citation

Ebnabbasi, Khabat, "UWB Antennas for Medical Imaging" (2009). *Theses and Dissertations - UTB/UTPA*. 1009.

https://scholarworks.utrgv.edu/leg_etd/1009

This Thesis is brought to you for free and open access by ScholarWorks @ UTRGV. It has been accepted for inclusion in Theses and Dissertations - UTB/UTPA by an authorized administrator of ScholarWorks @ UTRGV. For more information, please contact justin.white@utrgv.edu, william.flores01@utrgv.edu.

UWB ANTENNAS FOR MEDICAL IMAGING

A Thesis

by

KHABAT EBNABBASI

Submitted to the Graduate School of the
University of Texas Pan-American
In partial fulfillment of the requirement for the degree of

MASTER OF SCIENCE

June 2009

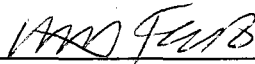
Major Subject: Electrical Engineering

Copyright 2009 Khabat Ebnabbasi
All Rights Reserved

UWB ANTENNAS FOR MEDICAL IMAGING

A Thesis
by
KHABAT EBNABBASI

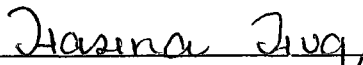
Approved as to style and content by:



Dr. Heinrich Foltz
Associate Professor of Electrical Engineering
Chair of Committee



Dr. Junfei Li
Associate Professor of Electrical Engineering
Committee Member



Dr. Hasina Huq
Assistant Professor of Electrical Engineering
Committee Member

June 2009

ABSTRACT

Khabat, Ebnabbasi, UWB Antennas for Medical Imaging. Master of Science (MS), June, 2009, 72 pp., 4 tables, 50 figures, 29 references.

Ultra-Wide Band (UWB) Microwave for imaging applications; especially in the medical field, is a new method to overcome the inherent invasive features of X-ray imaging. In this work a new systematic and detailed design for the Tapered Slot Antenna (TSA) as a UWB antenna in microwave imaging systems for medical applications is presented. Among TSAs, the Vivaldi antenna was selected and the reasons to replace the horn antenna imaging systems are illustrated. In the first chapter the previous designs for microwave imaging and the outline of this work are given, Chapter Two covers the design of the Vivaldi antenna's different parts design by concentration on previous researches, the third chapter presents the antenna design for this project, Chapter Four a method based on a closed form equation to design the antenna taper for reduced reflection is presented, the fifth chapter is a method to design the Vivaldi antenna taper to penetrate tissue like objects, and in the last chapter the UWB performance of the designed Vivaldi antenna and its impulse response are analyzed. In this work the theoretical designs are verified experimentally and the results and design justifications are provided for each part.

DEDICATION

My master studies results and completion would not have been possible without great advices, supports and kind cooperation of my advisor, Dr. Heinrich Foltz. I appreciate that and dedicate this thesis to him, and also my mother, Eran, and my father, Mitellib, in Kurdistan motivated and supported me by all means to accomplish this degree.

ACKNOWLEDGMENT

Opportunities to appreciate and remind those who play an important role in our life toward successes are few. So, I am delighted to take this time to appreciate my best teacher, till now, Dr. Heinrich Foltz for his support and respectable and didactic manner to deal with difficulties arising in research and non-experienced works. He trusted in and supported me to join his research activities. And during my study at UTPA his patience was sacred for me; especially his tolerance for my long time visa process and clearance period which is necessary for Iranian residents. Without any doubt, his recommendations many times led to come over many obstacles in my research work. Not only in research, but also in courses I took with him like RF circuits he taught us so many practical points. Even when I asked him to support me to participate in RF power amplifier design for student competition in MTT-S, 2009; although it wasn't the research with financial support and the laboratory didn't have good and development instruments to check our designs, he well received and in fact he was big help to get the considered results. So, let me say: Thank you very much for your patience and kindness.

And I would also like to thank my parents in Kurdistan for their support and their advice to motivate me; especially when I was new in USA and knew few people.

Other committee members Dr. Li and Dr. Huq both had great points in my thesis defense session. I hereby thank both of them and Laleh Asgharian for the thesis revision.

TABLE OF CONTENTS

	Page
ABSTRACT.....	iii
DEDICATION.....	iv
ACKNOWLEDGMENT.....	v
TABLE OF CONTENTS.....	vi
CHAPTER 1.A REVIEW ON MICROWAVE IMAGING SYSTEMS.....	1
1.1 Previous Works.....	2
1.2 This Work Design.....	5
1.3 The Design Advantages and Disadvantages.....	8
1.4 Aims and Significance.....	8
CHAPTER 2.ANTENNA PART OF SCANNING SYSTEM.....	9
2.1 Vivaldi Antenna Parameters Design.....	10
2.1.1 Feeding and Transition.....	10
2.2 Circuit Model for Transition.....	14
2.3 Micro-Strip and Coax Feeding Comparison.....	16
2.4 Slot-Line.....	17
2.5 Non-Conductor Board.....	21
2.6 Summary.....	22
CHAPTER 3.ANTENNA DESIGN.....	23
3.1 Antenna Parameters.....	23

3.2 The Non-Conductor Board Outline.....	24
3.3 Micro-Strip Design.....	24
CHAPTER 4.VIVALDI ANTENNA TAPER DESIGN.....	29
4.1 Introduction.....	30
4.2 Design Approach.....	30
4.3 Step Impedance Calculation.....	31
4.4 Smoothing.....	33
4.5 Experimental Results.....	35
4.5.1 Dimensions and Design Parameters.....	35
4.5.2 Impedance Bandwidth.....	38
4.5.3 Radiation Patterns.....	40
4.6 Conclusions.....	49
CHAPTER 5.VIVALDI ANTENNA TAPER DESIGN TO PENETRATE TISSUE LIKE OBJECTS.....	50
5.1 Impedance Calculation.....	51
5.2 Smoothing.....	54
5.3 Experimental Results.....	54
CHAPTER 6.UWB PERFORMANCE OF VIVALDI ANTENNAS.....	58
6.1 Introduction.....	59
6.2 Feed Structure.....	60
6.3 Antennas Used in This Experiment.....	60
6.4 Measurements.....	62
6.5 Frequency Domain Data.....	62

6.6 Time Domain Data.....	63
6.7 Conclusions.....	66
BIOGRAPHICAL SKETCH.....	72

LIST OF TABLES

	Page
Table I.....	14
Table II. Comparison of Taper Designs with Experimental Results.....	36
Table III. Antenna Parameters	61
Table IV. Impulse Response Parameters.....	65

LIST OF FIGURES

	Page
Fig.1-1 First Microwave Imaging Hardware Done by Bolomey.....	3
Fig.1-2 64 Antenna Circular Microwave Scanner.....	4
Fig.1-3 32 by 32 Antenna Circular Scanner.....	4
Fig. 1-4 Schematic of the Design.....	5
Fig. 1-5 (a) The Rotation Points of Transmitter and Receiver and Related Clocks of Steeper motor for One Rotate (b) The Matrix of Gathered Data for Transmitter and Receiver.....	7
Fig. 2-1 Vivaldi Antenna and Main Parts.....	9
Fig. 2-2 Coax-Slot Transition.....	10
Fig. 2-3 Simplified Equivalent Circuit for Coax Transition.....	11
Fig. 2-4 Different Sketches of Micro-strip (solid line) / Slot-line (dashed line) Transition He modeled the sketches as simple circuit models and showed that improved....	12
Fig. 2-5 Single Uniform Micro-strip Transition Parameters.....	12
Fig. 2-6 Equivalent Circuits for Transition (a) Soldered and (b) Virtual short	14
Fig. 2-7 Equivalent Circuit for Slot-line Micro-strip Transition.....	15
Fig. 2-8 Simplified Transition (a) Circuit Model (b) Selected Sketch and Coupling Section (c) Equivalent Circuit.....	15
Fig. 2-9 A sample Structure of Micro-Strip to Slot-line Transition with Circular Cavity and Radial Stub.....	17

Fig. 2-10 Antipodal Exponentially-TSA.....	18
Fig. 2-11 Different Types of TSA Taper (a) Exponential (Vivaldi) (b) Linear-Constant (c) Tangential (d) Exponential-Constant (e) Parabolic (f) Step-Constant (g) Linear (h) Broken-Linear.....	19
Fig. 2-12 Slot-Line Antenna (TSA) Taper Classes.....	19
Fig. 2-13 Vivaldi Antenna Taper Sections.....	20
Fig. 3-1 Vivaldi Antenna Parameters.....	24
Fig. 3-2 Micro-Strip Parameters for Radial Stub.....	25
Fig. 3-3 The Desired Design's Micro-Strip Values.....	28
Fig. 4-1 Multi-section Transmission Line.....	30
Fig. 4-2 Tapered Slot Antenna Modeled As a Series of Steps.....	32
Fig. 4-3 Points Used in Curve Fit Procedure.....	34
Fig. 4-4 Photograph of Micro-strip Input Matching Circuit. The Slot-line Crosses Horizontally on the Back Side Just Below the Apex of the Radial Stub.....	36
Fig. 4-5 Vivaldi Antenna the Example Shown is a Gaussian Fit to a Stepped Design....	36
Fig. 4-6 Measured VSWR for Exponential and Gaussian All-Points Curves.....	38
Fig. 4-7 Measured SWR for Exponential Gaussian, and Cubic Spline fits to Midpoints.	39
Fig. 4-8 Measured VSWR for Exponential, Gaussian, and Cubic Spline Fits to Top Points	39
Fig. 4-9 Measured VSWR for Three Different Cubic Spline Fits.....	39
Fig. 4-10 Radiation Pattern, Exponential All Points Curve (Design #1) Left: H-plane, Right: E-plane.....	41

Fig. 4-11 Radiation Pattern, Gaussian All Points Curve (Design #2)	
Left: H-plane, Right: E-plane.....	41
Fig. 4-12 Radiation Pattern, Exponential Midpoints Curve (Design #3)	
Left: H-plane, Right: E-plane.....	42
Fig. 4-13 Radiation Pattern, Exponential Top Points Curve (Design #4)	
Left: H-plane, Right: E-plane.....	42
Fig. 4-14 Radiation Pattern, Gaussian Midpoints Curve (Design #5)	
Left: H-plane, Right: E-plane.....	43
Fig. 4-15 Radiation Pattern, Gaussian Top Points Curve (Design #6)	
Left: H-plane, Right: E-plane.....	43
Fig. 4-16 Radiation Pattern, Cubic Spline fit to Bottom Points (Design #7)	
Left: H-plane, Right: E-plane.....	44
Fig. 4-17 Radiation Pattern, Cubic Spline fit to Midpoints (Design #8)	
Left: H-plane, Right: E-plane.....	44
Fig. 4-18 Radiation Pattern, Cubic Spline fit to Top Points (Design #9)	
Left: H-plane, Right: E-plane.....	45
Fig. 4-19 Example Cross-Polarization Patterns Gaussian Midpoints (Design #5) Left: H-plane, Right: E-plane.....	45
Fig. 4-20 Gain vs frequency for the different taper fits: (a) Exponential all points ,(b) Gaussian all points ,(c) Exponential midpoints,(d) Exponential top points ,(e) Gaussian midoints,(f) Gaussian top points, (g) Cubic Spline bottom points ,(h) Cubic Spline midpoints,and (i) Cubic Spline top points.....	47

Fig. 4-21 Experimental Fabricated for Different Taper Fit Over The Calculated Steps.....	48
Fig.5-1 Final Conformal Mapping of Whole Layers of Slot-Line.....	51
Fig.5-2 Selected Structure for Empirical Verification.....	55
Fig.5-3 Antenna Practical Example.....	55
Fig.5-4 VSWR Results.....	56
Fig.5-5 Transmission Results.....	57
Fig. 6-1 Transfer Function Magnitude.....	63
Fig. 6-2 Impulse Responses.....	64
Fig. 6-3 Impulse Responses.....	65

CHAPTER 1

A REVIEW OF MICROWAVE IMAGING SYSTEMS

In this chapter we present the theory behind design of an Ultra Wide Band (UWB) scanning system for medical imaging, first designed in the 1970s, analyzing and comparing its features as it has developed over time. The purpose of the set-up is to detect Electromagnetic (EM) properties of body tissues for medical purposes, such as malignant tumor recognition. The motivation behind our choice of this method is avoid the detrimental effects of X-rays as an ionizing method when used as a medical diagnostic tool. Microwave imaging is totally non-invasive and differentiates the objects by their dielectric constant which varies for different in-vivo tissues, but X-ray imaging is based on the density of the material and its obtained contrast is less than the dielectric constant recognition. The challenging part of hardware in hardware development is improvement of the device sensitivity improvement because the wave propagation is made complicated by complexity of body tissues.

Previous microwave imaging and detection methods [1]-[5] faced problems like leakage between transmitter antenna and receiver, complexity, number of antennas required, and limited frequency range. This work's objective is to make an effort to overcome these difficulties.

1.1 Previous Works

The hardware used for microwave scanning approaches can be classified in three main categories including set-ups performing in frequency domain methods, time domain methods and radar techniques. To reconstruct the data collected by the hardware, software is required which is based on one of several algorithms. Depending on the application different methods are used such as diffraction tomography and non-linear iterative algorithms. The main software challenge faced is the non-linear behavior of microwave scattering which requires complicated mathematical and numerical methods to reconstruct the image.

In this section we focus on the frequency domain approach. This system was first used by Bolomey in 1980s [1] as shown in Fig.1-1. It included two horn antennas in front of each other with a water tank in between. The object was immersed in the water which has a dielectric constant close that of human tissue. To distribute the scattered wave to the receiver a dipole antenna series on a plane matrix is placed on the tank in front of the receiver. The number of dipole antennas used in this work was 1024 with the modulation frequency of each antenna being 200 KHz. The qualitative images in this method have been reported with at a rate of 15 images /sec.

To improve images quality the hardware was developed in a way produce a circular microwave camera, shown in Fig. 1-2, which was able to do electrically multi view measurements without mechanical movements. The frequency used here was 2.45 GHz. This system used 64 horn antennas arranged in a circle and the way it worked was that one antenna served as a transmitter and 63 antenna served to receive the scattered wave in all the various directions.

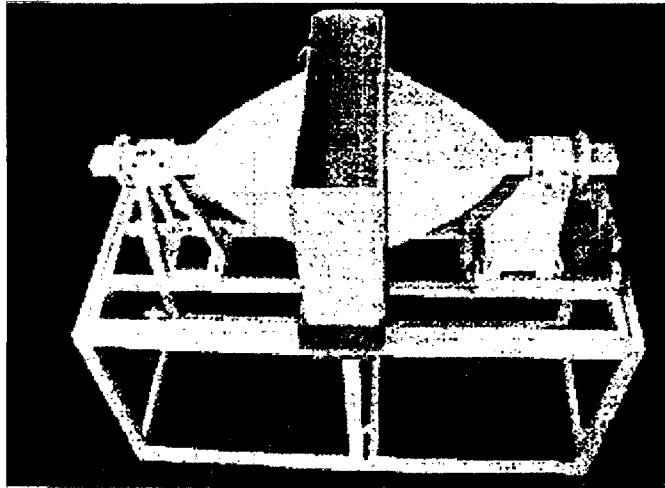


Fig.1-1 First Microwave Imaging Hardware Assembled by Bolomey [1]

To electrically switch to the next transmitter a multiplexer was required to be designed at a frequency of 2.45 GHz which turned out to be a big challenge. That was why the antennas were divided into four 1x16 multiplexers and then they are connected to T/R equipment through a 2-4 switching matrix. Besides complicated hardware, the system had two problems including leakage between the transmitter and receiver and isolation which was tried to be resolved by using low frequency modulation. The rate of imaging used in this method was around 21 images /sec. The system took a mere 3 seconds for each imaging cycle involving 64 antennas; however to reduce noise in the measurement process required 45 seconds per cycle. Although the imaging rate had been improved in this system, it was achieved by more complicated mechanical and electrical hardware, yet channel isolation remained drawback.

The other system, given in Fig.1-3, which was implemented by Semenov and his co-workers operating at the same frequency, was a 32 by 32 circular antenna system and was an attempt to reduce the hardware requirements, i.e. the number of antennas required

and proposed a way to overcome the channel isolation between transmitter and receiver which was a result of alternating the antennas [3]. So, in this way 32 antennas only will play the transmitter antenna role and 32 the receiver using separate channels.

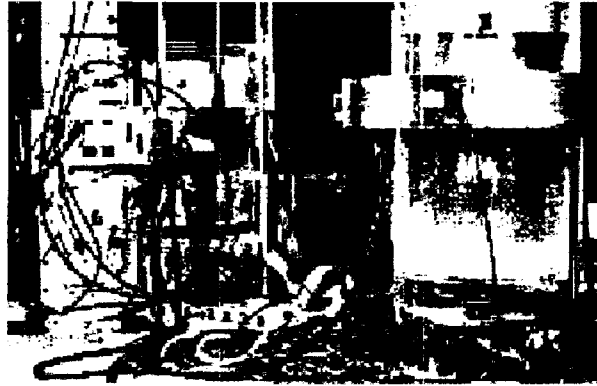


Fig.1-2 64 Antenna Circular Microwave Scanner [29]

Some other prototypes were developed to obtain a large number of images with improved quality and higher image rates than ones obtained using previous methods such as clinical circular scanners by Meany *et al* [5] and 434 MHz circular scanners developed by Geffrin *et al* [4].

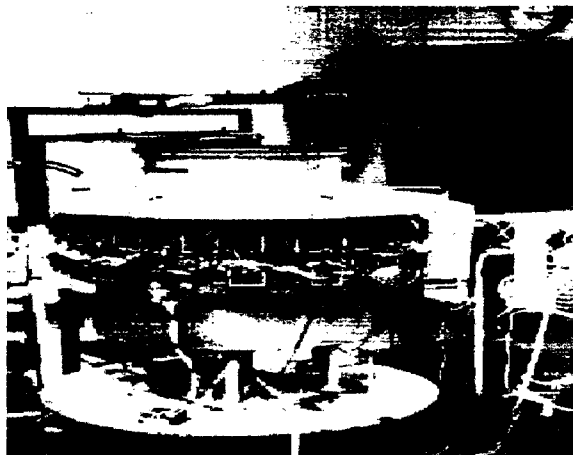


Fig.1-3 32 by 32 Antenna Circular Scanner [3]

In the Meany system the frequency range was 300-1100 MHz and only 8 antennas were applied which included four transmitting wave guide antennas and four monopole antennas. They tried to use a wide frequency range in order to find the optimum frequency suitable to their application. Geffin's method consisted of 64 antennas and was designed to scan entire human body.

1.2 The Experimental Design

As demonstrated, previous microwave imaging and detection methods [1]-[5] faced some major problems such as: leakage between transmitter antenna and receiver, complexity, number of antennas required, and limited frequency range. This work's objective is to make an effort to overcome these difficulties.

The goal of our research was to try to find a method or design a structure to solve the above mentioned problems which led to a design based on a mechanical rotary system with only two antennas. To increase the antenna coupling with the object a special kind of TSA or Vivaldi antenna was selected as a solution. This system uses analogous motion to cover the object in its entire range. Fig. 1-4 shows the schematic of the design.

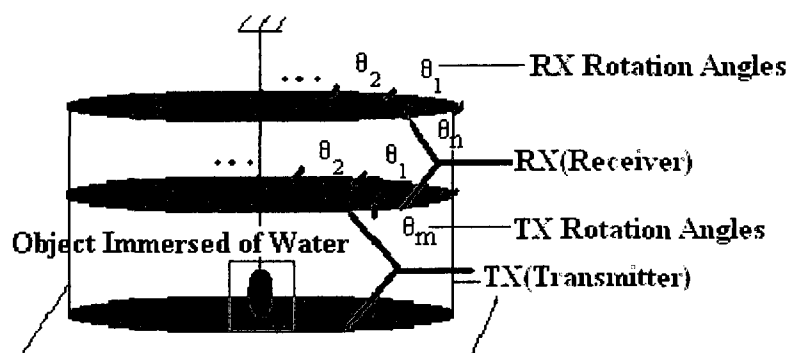


Fig. 1-4 Schematic of the Design

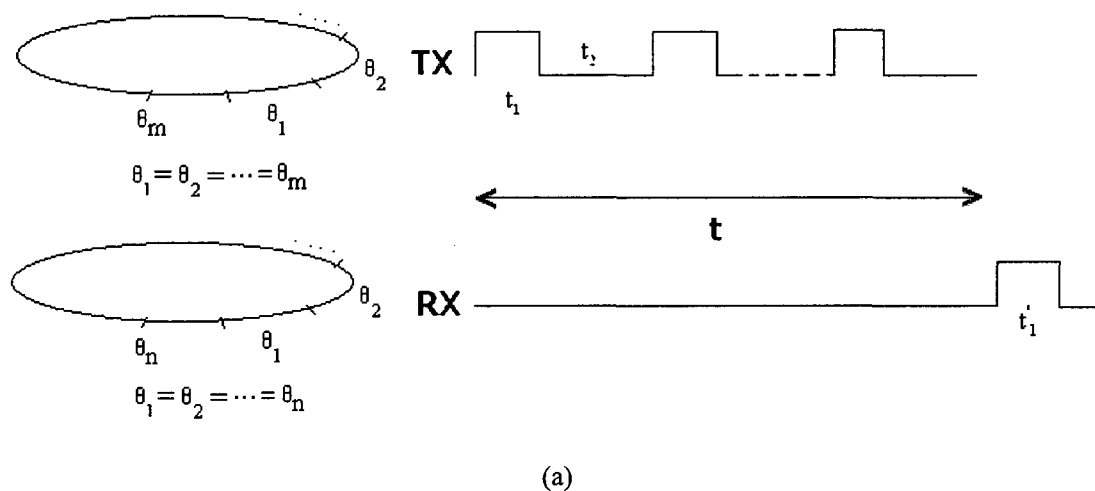
The object is fixed and the receiver or transmitter will rotate around the object to allow bi-static detection with any incident and return angle. The transmitter can rotate using a stepper motor through a given angle and the receiver will be fixed to gather the scattered data for a complete rotation of the transmitter. Then the receiver will rotate for a given angle and the same process will repeat for the transmitter and for the new position of the receiver. A schematic picture is given in Fig. 1-5.

For a detailed process of rotation the following steps can be followed:

- 1- TX (Transmitter) or RX (Receiver) rotates through a pre-determined angle. Here it is supposed that TX rotates first and RX is fixed. So, the TX rotation angle is θ_1 which can be achieved by a stepper motor fed by a clock set to High level for t_1 seconds and then set to Low level t_2 seconds. The angle θ_1 is synchronized to the time interval t_1 as shown in Fig.1-5 (a).
- 2- The previous step is repeated for TX and it is rotated through $\theta_2, \dots, \theta_m$. During TX rotation in this way, RX is fixed. Just as TX sweeps θ_m and stops there for t_2 seconds, RX rotates for θ_1 , which can be done by feeding the RX stepper motor for t_1 seconds. Then RX will stop there and again the same process repeats for TX as in steps 1 and 2.
- 3- This process is completed when RX sweeps through rotation path for θ_n .

This process for one rotation cycle of TX is given in Fig.1-5 (a) which takes t seconds. The depicted loops are the paths swept by TX and RX.

The data thus collected forms a $m \times n$ matrix, given in Fig.1-5 (b) such that the gathered scattered data in at a specific frequency as TX rotates and RX is fixed are placed in the rows of matrix, and those obtained when TX is fixed and RX rotates are placed in the matrix columns. In Fig. 1-5 (b) T and R denote transmitter and receiver intensities respectively.



RX is Fixed and TX Rotates
→

↓ TX is Fixed and RX Rotates

$$\begin{bmatrix} T_1 R_1 & T_2 R_1 & \dots & T_m R_1 \\ T_1 R_2 & T_2 R_2 & \dots & T_m R_2 \\ \vdots & \vdots & \ddots & \vdots \\ T_1 R_n & T_2 R_n & \dots & T_m R_n \end{bmatrix}$$

(b)

Fig. 1-5 (a) The Rotation Angles of Transmitter and Receiver and the Associated Stepper Motor Clocks for One Rotation Cycle (b) The Matrix of Gathered Data for Transmitter and Receiver

1.3 Advantages and Disadvantages of The System Design

By using only two antennas, one serving as the transmitter and the other as the receiver, sweeping a round path, the channel isolation should be improved over previous systems. With better channel isolation a more precise image can be acquired.

The set-up is also more economic than previous systems because of the reduced number of antennas required and elimination of the MUX and electronic hardware. In addition Vivaldi antennas are economic than horn antenna.

The hardware requirements are reduced because there is no need to design switching boards for switching among antennas and no need to design a MUX board to gather data. The only hardware required are the antennas, electric stepper motors and the non-conducting material needed to cover the whole system.

The only disadvantage of our system is the time required to acquire data, which exceeds that of conventional methods, some of which required less than a minute.

1.4 Goals and Significance of Our Novel Design

Our first objective was to design an antenna that worked in the frequency range of 1-3 GHz with a VSWR less than 1.5 over the entire range as well as high coupling and less reflection at the object's surface which has been one of the most important challenges for our applications of interest. The antenna design and the method used to design the Vivaldi antenna taper is the subject of the chapters 2-3. In chapter 4 we cover the methods we use to improve penetration through tissue-like objects.

We chose to incorporate Vivaldi antenna in our system for several reasons

including high directivity, high BW range and high transmission coefficient, as well as their light weight.

CHAPTER 2

ANTENNA PART OF SCANNING SYSTEM

The TSA (Taper Slot Antenna), "Taper-Notch Antenna" or "Flared-Slot Antenna", is a member of the general class of end-fire traveling wave antennas and the Vivaldi antenna is a special type of TSA which includes a tapered slot on a thin layer of non-conductor material like FR-4 (PCB fiber), *mostly used in VHF range and <500MHz*, HiK or RT-Duroid, *mostly used in microwave applications*. This kind of antenna works over a wide range of frequencies has high gain, low side lobes and good directivity.

The Vivaldi antenna as shown in Fig.2-1 below includes three main parts:

- 1) Feeding and transition from micro-strip to slot-line
- 2) Slot-line: An open boundary structure which guides wave having appreciable energy stored outside the region of slot [10]-[11].
- 3) The non-conductor substrate.

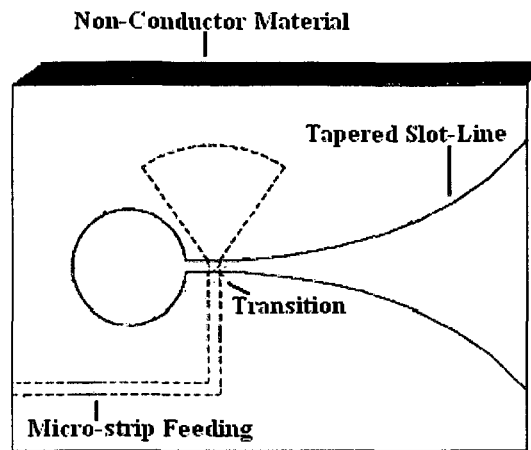


Fig. 2-1 Vivaldi Antenna and Main Parts

2.1 Vivaldi Antenna Parameters Design

The parameters and dimensions of each part are described subsequently.

2.1.1 Feed line and Transition

The antenna feed line and transitions are very important factors since they impact band width. The antenna can be fed by two methods: a) Coaxial Cable and b) Micro-strip.

a) Coax Feeding

In the first method, shown in Fig.2-2, the cable shield or outer conductor is soldered to the slot-line or ground plane and the core is bent perpendicular over the other part of the slot-line as close as possible. Knorr [6] showed the coax transition radiation is in the vicinity of the coax-slot transition and termination, and by moving a reflecting object around the antenna, around 30-60cm distance, a minor change is observed in VSWR, because of the open ended slot-line, while the shorted stub and micro-strip do not radiate. The simplified circuit model for a coax transition [6]-[7] is given in Fig. 2-3 where n is:

$$n = \frac{V(r)}{V_0} = \frac{\pi}{2} |k_c r H_1^{(1)}(k_c r)| \quad (2.1)$$

where
$$k_c = j \frac{2\pi}{\lambda} \left[1 - \left(\frac{\lambda'}{\lambda} \right)^2 \right]^{1/2} \quad (2.2)$$

$V(r)$ is voltage at radius r shown in Fig.2-3 (b) and V_0 is the voltage directly across the slot, λ' is the slot-line wavelength and

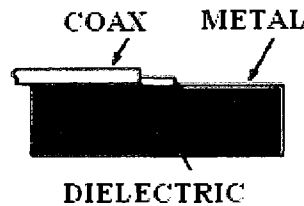


Fig. 2-2 Coax-Slot Transition

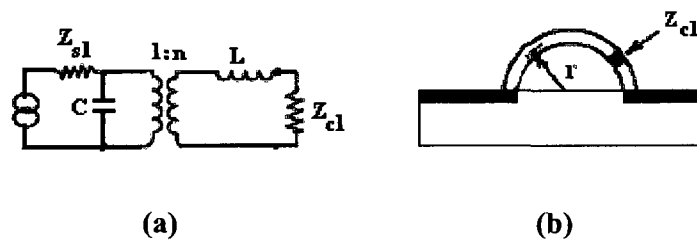


Fig. 2-3 Simplified Equivalent Circuit for Coax Transition

$H_1^{(1)}(k_c r)$ is the Hankel function. The capacitor C is the fringe capacitance at the open end of the slot which for typical applications is less than 1pF. The L is the self-inductance of a semi-loop of radius r and depending on the design is usually less than 1nH. There is no precise way to calculate these parameters, except by programming and varying them in reasonable limits to meet the experimental results [7], but Knorr [6] measured the L parameter by TDR (Time-Domain Reflectometer) which in their experiment was 0.61nH.

The coaxial radiation takes place in the vicinity of the cable-slot transition and if the cable is as close as possible to the slot, least reflection occurs and reflective objects have

least influence on that. So, the reflection depends upon the cable distance from the slot and the distance of reflector objects from the transition. For instance a reflector can impact it at 1-2 ft distance. The core of the cable diameter should be as low as possible to decrease the reflection.

For higher bandwidth the practical difficulty of this method is placing the coax directly across the slot. Otherwise the transition will lead to higher VSWR in the higher part of the frequency range.

(b) Micro-strip feeding

Schuppert [8] analyzed the micro-strip slot-line transition using transmission lines. His work included four different transition types as given in Fig.2-4.

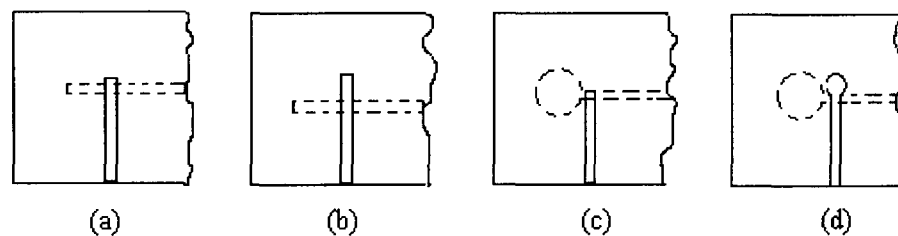


Fig. 2-4 Different Types of Micro-strip (solid line) / Slot-line (dashed line) Transitions [8]

He modeled the transitions as simple circuit models and showed that improved bandwidth resulted from (b) than from (a) by reactance compensation effect. He found that the circular shape provides also an improved flatness and the bandwidth is better in (c) than in (d).

He supposed two different circuit models as given in Fig. 2-6 for soldered and virtual short designs. In detail the micro-strip transition parameters are given in Fig. 2-5 which can be calculated [9] by formulas below which result from maximum power transfer at the center frequency:

$$l_s = (\lambda_s / 2\pi) \text{tg}^{-1}(z_{0s} / 2\pi f_0 L_{sc}) \quad (2-3)$$

$$l_m = (\lambda_m / 2\pi) \text{tg}^{-1}(1 / 2\pi f_0 z_{0m} C_{0m}) \quad (2-4)$$

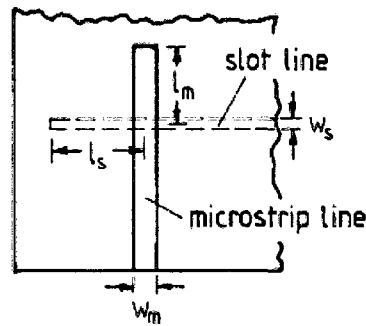


Fig. 2-5 Single Uniform Micro-strip Transition Parameters [9]

λ_s : Slot-line wave-length

z_{0s} : Slot-line characteristic impedance

λ_m : Micro-strip wave-length

z_{0m} : Micro-strip characteristic impedance

f_0 : Center frequency.

The L_{sc} and C_{0m} parameters are shown in Fig. 2-6 and are slot-line end inductance and micro-strip open circuit end capacitance respectively. Their values can be obtained by numerical methods [10]. In a slot-line significant end effect exists when it is shorted and in the shorted slot end effect investigation, the short position is observed as a small fraction of the wavelength beyond the end of the slot which verifies that the reactance is inductive [10]. The shorted slot reactance inductance is determined by VSWR measurements.

Other methods are used to analyze the transition such as MOM, or Method of Moments, and in their formulation Green's function for grounded dielectric substrate is used [12]. In this work the transition given in Fig. 2-4 (d) was used.

Silvester and Benedek [13] provided a closed form equation for end effect capacitance. It was based on the charge distribution near open circuit micro-strip end and was formulated by computational methods.

$$C = \exp[\ln 10 \sum_{i=1}^5 c_i(\epsilon_r)(\log w/h)^{i-1}] \quad (2-5)$$

Where c_i is placed by the Table I: in the paper the techniques are described in more detail. The specific cases for $\epsilon_r=1$ and 2.5 are in Table I:

Table I

$i \backslash \epsilon_r$	1	2.5
1	1.110	1.295
2	-0.2892	-0.2817
3	0.1815	0.1367
4	-0.0033	-0.0133
5	-0.0540	-0.0207

2.2 Circuit Model for Transition

In different papers special types of circuit models have been proposed and analyzed. Schuppert [8] had a microwave model as given in Fig. 2-5, which is quite similar to what can be found in [9], Fig.2-7, a lumped element model. In the model the slot-line short inductance and micro-strip open circuit capacitance have been shown clearly.

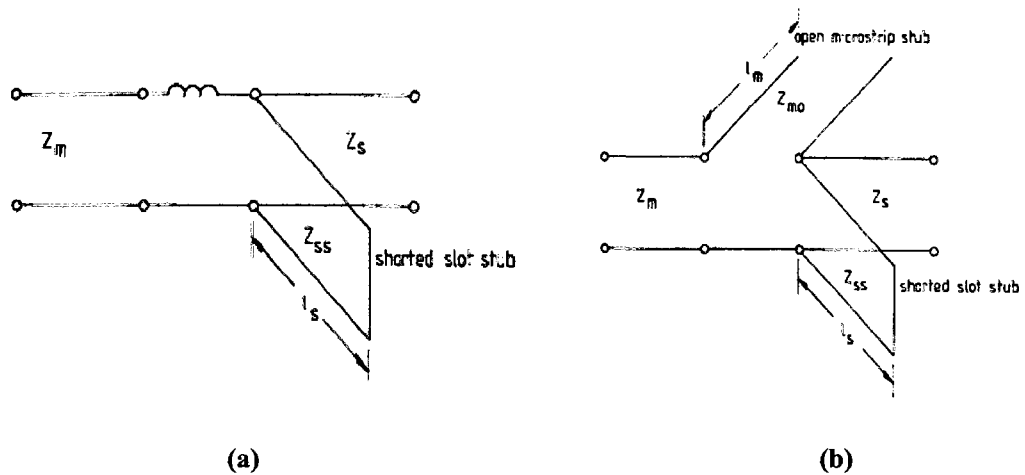


Fig. 2-6 Equivalent Circuits for Transition (a) Soldered and (b) Virtual short [8]

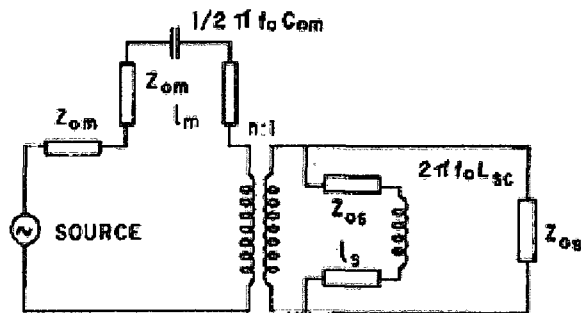


Fig. 2-7 Equivalent Circuit for Slot-line Micro-strip Transition [9]

Fig.2-8 is the circuit model for the transition which is used for the antenna design in this work and thesis. As subsequently shown, the slot-line on one side extends a quarter slot wavelength beyond the micro-strip, on the other side; the micro-strip extends a quarter micro-strip wavelength [14]. This method provides a closed form equation to design parameters and a more precise design than previous methods which required computational and complex math calculation.

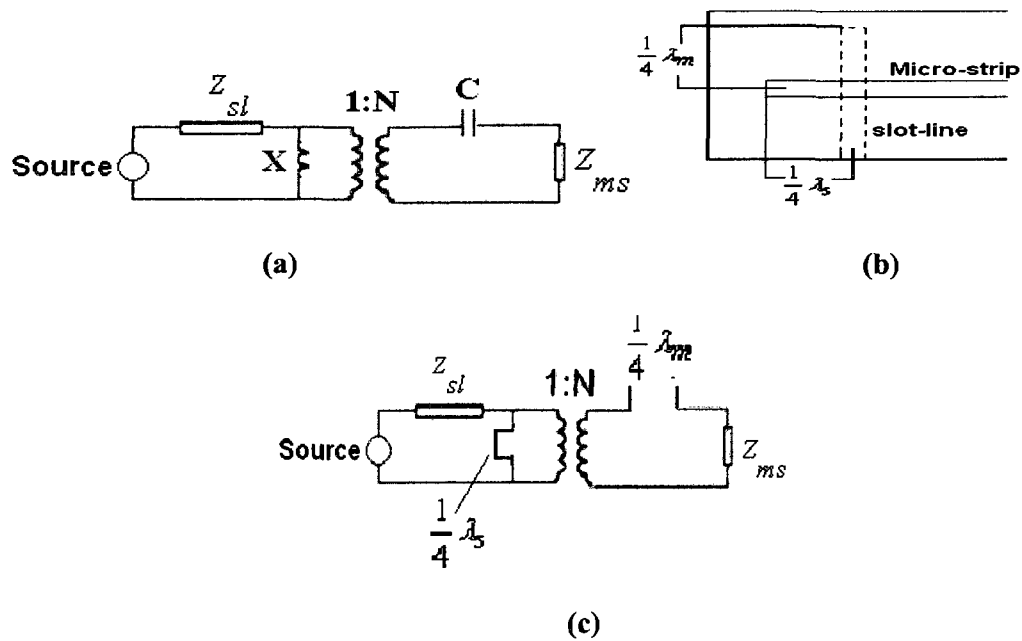


Fig. 2-8 Simplified Transition (a) Circuit Model (b) Selected Sketch and Coupling Section (c)

Equivalent Circuit [14]

C: micro-strip open circuit equivalent capacitance

X: slot short equivalent reactance

Perfect impedance match between the micro-strip and slot can be achieved if the susceptance looking into the shorted slot stub and the reactance looking into the open circuited micro-strip stub are both zero ($B_{sl}=0$ and $X_{ms}=0$)

Then
$$Z_{ms} = N^2 Z_{sl} \quad (2-6)$$

where:
$$N = \cos 2\pi \frac{D}{\lambda} u - \cot(q_0) \sin 2\pi \frac{D}{\lambda} u \quad (2-7)$$

and:
$$q_0 = 2\pi \frac{D}{\lambda} u + \tan^{-1} \left(\frac{u}{v} \right) \quad (2-8)$$

$$u = \left[\epsilon_r - \left(\frac{\lambda}{\lambda_0} \right)^2 \right]^{1/2}, \quad v = \left[\left(\frac{\lambda}{\lambda_0} \right)^2 - 1 \right]^{1/2} \quad (2-9)$$

Where λ , λ' and D are the free space wave length, the slot wave length and the substrate thickness respectively.

2.3 MicroStrip and Coax Feeding Comparison

From the manufacturing point of view the micro-strip transition is more stable than the coax one; especially mobile systems or applications, where the antenna is required to rotate or move through a path like in scanning systems. The reason is that the coax must be fixed perpendicular over and in the vicinity of the slot. So, by using a micro-strip we can make sure there is no change in the physical situation of the transition where in coax we can not.

From another view good VSWR over the frequency band width is achieved using a micro-strip. A sample micro-strip to slot-line transition structure is given in Fig.2-9.

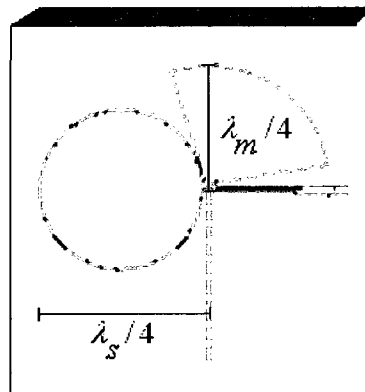


Fig. 2-9 A Sample Structure of Micro-Strip to Slot-line Transition with Circular Cavity and Radial Stub

In this work and all designs in this experiment the transition given in Fig. 2-9 is used. Most previous work in the literature had better experiences with this kind of structure.

2.4 Slot-Line

The impact of the slot-line taper on antenna performance in an array; especially on band width was studied by Shin and Schaubert [15], and they found out that the improvement must be systematic which includes the transition, slot-line and the strip-line stub and slot-line cavity. In their study which mostly focused on the slot-line it was shown that the lower end of the frequency range can be lowered by increasing the antenna resistance which results from changing the parameters. Here, the resistance is affected by the combination of the slot-line cavity and taper radiator.

The effect of curvature and tapered profile were studied by Lee and Simsons [18] and their practical experiences indicated significant impact on the gain, beam width, frequency band width and cross-polarization of the TSA. The effect of taper profile on directivity depends on the radius of curvature such that the half power beam width (HPBW) for the E-plane increases when the radius decreases while the opposite is true for the H-plane. Decrease in radius leads to bandwidth reduction.

The curvature also affects the antenna parameters and generally degrades the E-plane, but improves the H-plane directivity. However E-plane cross polarization will increase. In most of the experiments the exponential taper has been used for the slot-line [15]-[18]. In few works some other kinds of tapers have been proposed like the antipodal TSA-Vivaldi [19] antenna which is also inherently exponential, but with a especial shape given in Fig.2-10. Different kinds and classes of Vivaldi antenna taper have been offered in different papers Some of these are shown in Fig. 2-11 and can be classified, Fig 2-12, in three main classes [20]: (1) Non-Linear Taper, like Vivaldi, Tangential and Parabolic,

(2) Linear Taper Slot Antenna (*LTSA*) and (3) Constant width Slot Antenna (*CWSA*) like (b), (d) and (f).

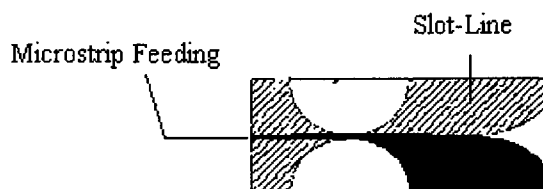


Fig. 2-10 Antipodal Exponentially-TSA [19]

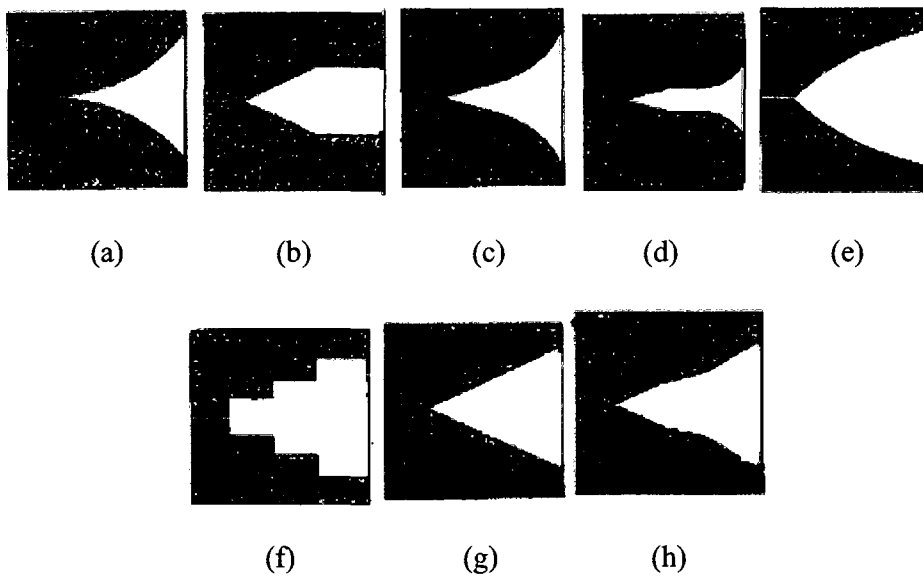


Fig. 2-11 Different Types of TSA Taper (a) Exponential (Vivaldi) (b) Linear-Constant (c) Tangential (d) Exponential-Constant (e) Parabolic (f) Step-Constant (g) Linear (h) Broken-Linear [20].

In these kinds of Antennas the radiation is along the antenna structure and the phase velocity is less than the speed of light in free space with a substrate and equal to the speed of light without a substrate or with air dielectric [20]. As shown in Fig.2-12 the main lobe is in the end-fire direction at the widest end side of the taper. The antenna has a symmetric radiation pattern with side lobes.

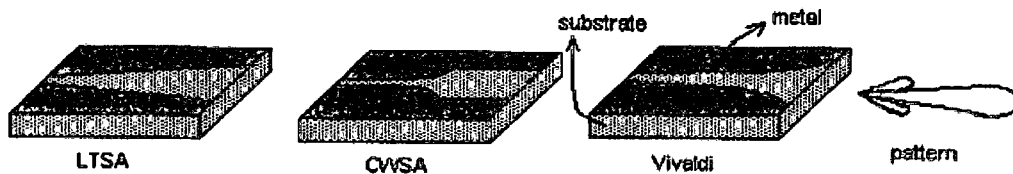
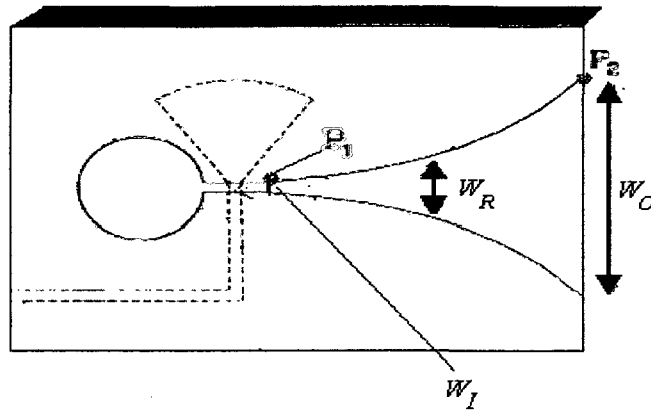


Fig. 2-12 Slot-Line Antenna (TSA) Taper Classes

The focus of this work is on the Vivaldi antenna for its performance in comparison to other kinds of TSAs including higher gain, wider band width and less reflection. The Vivaldi antenna and the experimental results for the first time were published by P.J. Gibson [16]. In that work using 3-dB beamwidth and radiation pattern empirical results it was shown that using an exponential taper, significant gain, frequency band width, linear polarization and constant gain versus frequency can be obtained which are significant elements in practical applications such as communication and imaging systems.

In Vivaldi antenna a section or a part of the taper radiates where edges are separated by $\lambda/2$, where λ is the free space wavelength since the energy of a traveling wave is confined when the separation between the edges is small. In Fig.2-12 it is shown as W_R . W_I is the input width where the taper begins to separate from each other at the start points and W_O is the output or end point widths.



$$\begin{cases} W_I \leq W \leq W_R; \text{Propagation Area} \\ W_R \leq W \leq W_O; \text{Radiation Area} \end{cases}$$

Fig. 2-13 Vivaldi Antenna Taper Sections

The Slot-line has an exponential taper and that is what, as described above, distinguishes the VA from other kinds of TSAs. It is defined by $y = A_1 e^{Rx} + A_2$ where A_1 and A_2 are constants and R is the opening rate which determines the beam width, in other words, if the tapers are opening very fast then the beam width will be independent almost over the entire frequency range [16].

If we suppose the $P_1(x_1, y_1)$ and $P_2(x_2, y_2)$, given in Fig.2-13, as the beginning and end points then:

$$A_1 = \frac{y_2 - y_1}{e^{Rx_2} - e^{Rx_1}} \text{ and } A_2 = \frac{y_1 e^{Rx_2} - y_2 e^{Rx_1}}{e^{Rx_2} - e^{Rx_1}}$$

The VA essentially is frequency independent, since at every wave length a portion of the antenna radiates and when the wave length varies, this section changes which is scaled in size in proportion to the wave length [17]. Theoretically the bandwidth of VA is infinite, but the substrate is a limiting factor and the bandwidth is not limited only by the finite dimension but also by the transition from micro-strip to slot-line. So, two main

factors determine the BW: one is the substrate and the taper shape and the other is the transition from main feeding to slot-line. By using the micro-strip method for feeding the impedance matching will be difficult which is why transition limits the BW.

2.5 Non-Conductor Board

The effect of the board permittivity, especially on infinite arrays was analyzed by Sreenivas and Schaubert [22]. The performance was studied by computing the input impedance of a single antenna in an array by full wave and MOM (Method of Moments) methods. They found out that dielectric permittivity plays an important role in the frequency and impedance wide-band performance of such arrays and they are in direct proportion to the permittivity. However higher permittivity beyond a certain range will result in performance loss at high frequency.

2.6 Summary

In this chapter the Vivaldi antenna and its main parts like the micro-strip and slot-line were illustrated, and a brief review of the work structure was provided by doing an in depth study of previous related work. The results from previous work were presented comparing their methods with respect to the bandwidth, gain, directivity, and reflection, and highlighting their features and drawbacks. These will be the basis of decisions for the design which will be presented in the next chapter.

CHAPTER 3

ANTENNA DESIGN

In this chapter the method used to design the Vivaldi antenna is presented. The method is based on lessening the reflection for each part of antenna. We also provide an overview of the slot-line taper design, but cover the subject more in depth in the next chapter, where we present and new method based on impedance.

In every step the parameters for the desired antenna are provided. The antenna is to be designed for 1-3GHz frequency range and will be implemented on a board with a dielectric constant of 6.15 and a thickness of 1.27mm.

3.1 Antenna Parameters

In Fig.3-1 the parameters of Vivaldi Antenna are presented which can be calculated using the given values for the dielectric constant, board thickness, frequency range, and so on. In this work the antenna is supposed to consist of a circular cavity and radial

In some papers the Method of Moment (MOM) has been used to calculate the parameters, but here closed form equations are applied. In the following section we present our calculation.

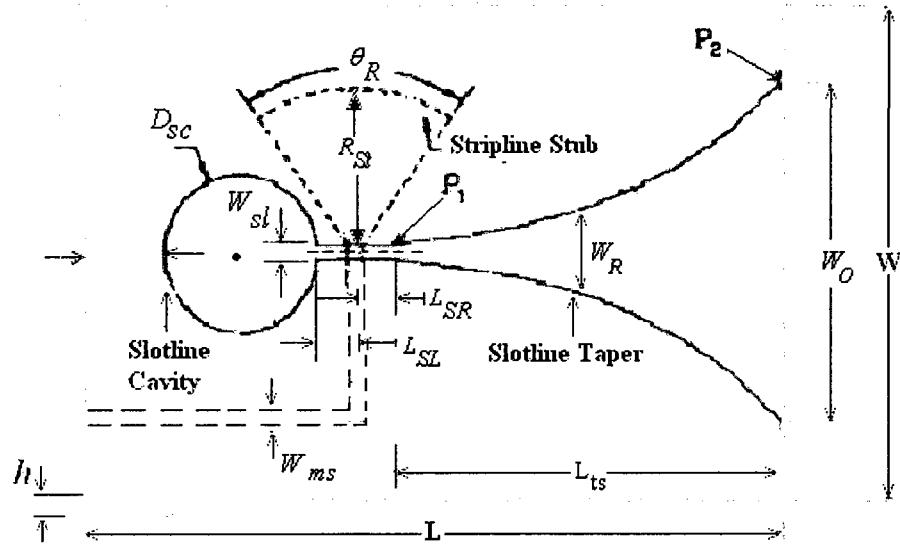


Fig. 3-1 Vivaldi Antenna Parameters

3.2 The Dimensions of the Non-Conducting Board

The goal in this design is to achieve a wide-band performance. And for a radiation traveling mode the optimum value for board length should exceed the wavelength of free space at lower frequency range [20] and width should be greater than the half of the wave-length of free space [23].

So, as illustrated in Fig.3-1:

$$\begin{cases} L > \lambda \\ W > \lambda/2 \end{cases}; \text{ where } \lambda \text{ is the free space wave-length at the lowest frequency} \quad (3-1)$$

3.3 Micro-Strip Design

The micro-strip parameters includes: Radial stub angle, θ_R , and length, R_{St} , micro-strip width, W_{ms} , and micro-strip length, L_{ms} .

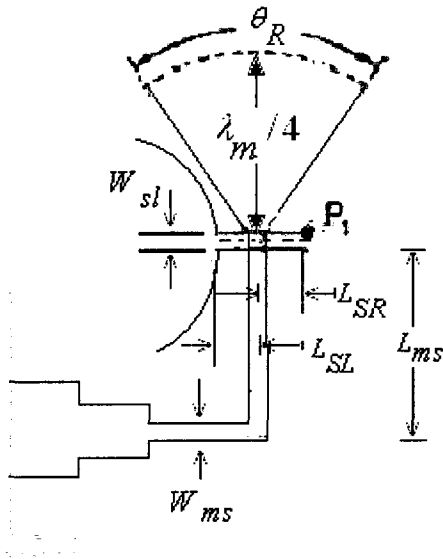


Fig. 3-2 Micro-Strip Parameters for a Radial Stub

To obtain W_{ms} value, it is required to calculate the slot-line impedance at the transition point. The slot-line impedance can be found using the closed form formulas provided in the relevant reference books for slot-line [24]. In the equations, some ranges or pre-conditions (initial values) for some parameters like the dielectric constant, the free space wave length and the slot-width at the transition point are given. Only if those pre-conditions are satisfied, can the parameters be incorporated in the design calculations. For instance, after selection of the non-conducting material an appropriate value should be determined for W_{sl} , the slot width, to meet the parameter's allowed range.

The board we use in our work was a RO-3206 RT-Duroid from Rogers company with $\epsilon_r=6.15$ and $h=1.27\text{mm}$. The width of this board, W_{sl} is supposed to be 0.5mm. The reason for our choice of this board will be described in the next chapter where the method used to design the taper is presented.

In this case:

$$\begin{cases} 3.8 \leq \epsilon_r = 6.15 \leq 9.8 \\ 0.0015 \leq W_{sl} / \lambda_0 = 0.0033 \leq 0.075 \\ 0.006 \leq h / \lambda_0 = 0.008 \leq 0.06 \end{cases} \quad (3-2)$$

So, the slot-line impedance is [24]:

$$\begin{aligned} Z_{0s} = & 73.6 - 2.15 \epsilon_r + (638.9 - 31.37 \epsilon_r)(W_{sl} / \lambda_0)^{0.6} \\ & + (36.23 \sqrt{\epsilon_r^2 + 41} - 225) \frac{W_{sl} / h}{(W_{sl} / h + 0.87 \epsilon_r - 2)} \\ & + 0.51(\epsilon_r + 2.12)(W_{sl} / h) \ln(100h / \lambda_0) \\ & - 0.753 \epsilon_r (h / \lambda_0) / \sqrt{W_{sl} / \lambda_0} \end{aligned} \quad (3-3)$$

The slot-line wave length formula versus free space wave length also has a closed form solution. The λ_0 in the formula represents the free space wave length and in this work is 15cm. The antenna is designed for 1-3GHz frequency range and λ_0 is the equivalent value for the average frequency. For the desired antenna the calculated values of Z_{0s} and λ_s are 84.0421 Ω and 99.51mm respectively.

As presented in the previous chapter, to have perfect impedance match for maximum power transition the shorted slot stub susceptance and the open micro-strip reactance should both be equal to zero. So,

$$Z_{ms} = N^2 Z_{sl} \quad (3-4)$$

where:

$$N = \cos 2\pi \frac{D}{\lambda} u - \cot(q_0) \sin 2\pi \frac{D}{\lambda} u \quad (3-5)$$

and:

$$q_0 = 2\pi \frac{D}{\lambda} u + \tan^{-1} \left(\frac{u}{v} \right) \quad (3-6)$$

$$u = \left[\epsilon_r - \left(\frac{\lambda}{\lambda_s} \right)^2 \right]^{1/2}, \quad v = \left[\left(\frac{\lambda}{\lambda_s} \right)^2 - 1 \right]^{1/2} \quad (3-7)$$

Where λ , λ_s and D are the free space wave length, the slot wave length and the substrate thickness respectively. For the desired antenna, $u=1.97$, $v=1.13$, $q=1.155$, $n=0.95$ and $Z_{ms}=75.56$.

$$Z_{ms} = \frac{\eta_0}{\sqrt{\epsilon_{eff}}} \left[\frac{W_{ms}}{h} + 1.95 \left(\frac{W_{ms}}{h} \right)^{0.172} \right]^{-1} \quad (3-8)$$

η_0 is the free space characteristic impedance and is equal to 120π .

Where:

$$\epsilon_{eff} = 1 + \frac{\epsilon_r - 1}{2} \left[1 + \frac{1}{\sqrt{1 + 10h/W_{ms}}} \right] \quad (3-9)$$

In formulas the only unknown parameter is the micro-strip width which can be easily calculated using MATLAB m-file programming and replacing the impedance and effective dielectric constant values.

The feeding will be connected to a 50Ω network analyzer connections. So, to match the micro-strip calculated value to 50 ohm a three-step a quarter wavelength micro-strip is designed. The middle step impedance is calculated such that

$$Z_{ms2} = \sqrt{Z_{ms1} Z_{ms3}} \quad (3-10)$$

For this design the middle step impedance is equal to 61.48 ohms. The same method is used to calculate the width of each step using formulas provided for computing micro-strip impedance. As mentioned before the length of each step as mentioned is $\lambda_{ms} / 4$ where

$$\lambda_{ms} = \frac{\lambda_0}{\sqrt{\epsilon_r}} \quad (3-11)$$

and in the objective design it works out 18.22mm.

The values for each step in the design are shown in Fig.3-3 where the widths are given in mm.

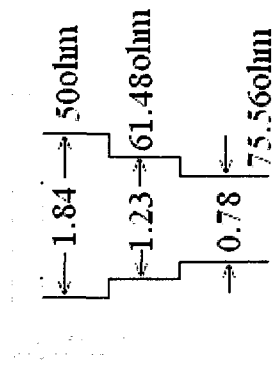


Fig. 3-3 The Desired Design's Micro-Strip Values

CHAPTER 4

VIVALDI ANTENNA TAPER DESIGN

A new method for the design of slot-line tapers for Vivaldi antennas is presented, which is based on closed-form equations. In this method the slot-line is modeled by a series of quarter-wave transformer sections. The step impedances are computed using closed-form Chebychev transformer design formulas, then different curves (exponential, Gaussian, and cubic spline) are fit to the steps. It is found that wider bandwidths are achieved using a cubic spline fit, compared to a conventional exponential taper. The validity of the method is verified through measurements of experimental designs for the 0.5 to 3.5 GHz range.

4.1 Introduction

The Vivaldi antenna [6] is a tapered slot antenna (TSA) with directional, endfire radiation. Its primary advantage is reasonably high gain (6-10 dB) and wide bandwidth combined with simple planar fabrication. When fed with a micro-strip, the impedance and gain bandwidth are determined by a number of factors including, among others, the slot taper. Several approaches have been used for the taper design, most of them exponential with a trial-and-error approach to determining the exponential rate. Oraizi and Jam [21] have presented a comprehensive optimum design based on a stepped approximation combined with numerical EM simulation; however, this approach requires significant computational effort. An alternate method for design of the slot-line taper given a desired size and center frequency is presented here, which is based on the design of slot-line stepped transformer. The approach uses closed-form formulas for synthesis of the steps and simple curve fits to derive the tapers, and yields results with over three octaves impedance bandwidth.

4.2 Design Approach

The design approach begins by considering a multi-section quarter-wave transformer design, as shown in Fig. 4-1.

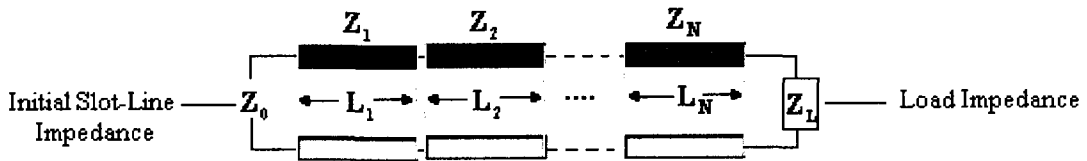


Fig. 4-1 Multi-section Transmission Line

Each section has a length $L_i = \lambda/4$, and the characteristic impedances Z_i follow the rule:

$$Z_i Z_{N+1-i} = Z_0 Z_L \quad (4-1)$$

for $i = 1, 2, \dots, N$, where N is the number of sections, and Z_0 is the initial slot line impedance at the feed point. The load impedance Z_L is taken to be very high ($Z_L \rightarrow \infty$) corresponding to a slot-line section with infinite width. The characteristic impedance of the intermediate steps is calculated by using Chebyshev transformer techniques. The characteristic impedances are then used to determine the slot width using standard formulas for slot-line impedance. For better performance, as we use the results from previous works done in this area to fit a curve, to the computed steps.

4.3 Step Impedance Calculation

The dimensional parameters for the design are defined in Fig. 4-2. The input specifications are the desired overall length L and width W for the entire antenna structure, and the desired center frequency f_0 . The choices for L and W as described in the previous chapter and are limited by the minimum frequency and should be greater than λ_0 and $\lambda_0/2$ respectively of the lowest frequency in free space. The slot-line portion of the Vivaldi antenna is modeled by N steps. The characteristic impedance of the initial strip-line section, Z_0 , is selected for convenience in fabrication and design of the micro-strip to slot-line transition, and is described as follows.

Since each step is one-quarter guide wavelength, the number of steps is calculated from the length as

$$N = 4 (L - L_{sl}) / \lambda_s \quad (4-2)$$

where λ_s is the slot-line guide wavelength, and L_{sl} is the distance from the board edge to the first step and $L - L_{sl}$ is equal to L_{ts} shown in Fig. 3-1. L_{sl} is set to one-quarter of the free space wavelength λ_0 in order to give room for the circular terminating cavity and some margin between the cavity and board edge. The guide wavelength depends on the

slot width, which varies at each step and is initially unknown. However, as an initial estimate for the purpose of computing N , it can be taken as the guide wavelength for the first step.

The characteristic impedance for the succeeding steps is set using the following procedure:

$$T_N(x_0) = \left(\frac{Z_L - Z_0}{Z_L + Z_0} \right) \frac{1}{\Gamma_m} \quad (4-3)$$

where $T_N(x_0)$ is the N -th order Chebychev polynomial and Γ_m is the maximum tolerable reflection response in the passband. Then one computes

$$x_0 = \cosh \left[\frac{1}{N} \cosh^{-1} (T_N(x_0)) \right] \quad (4-4)$$

and

$$x_n = \cos \left((2n-1) \frac{\pi}{2N} \right); \text{ for } n = 1, \dots, N. \quad (4-5)$$

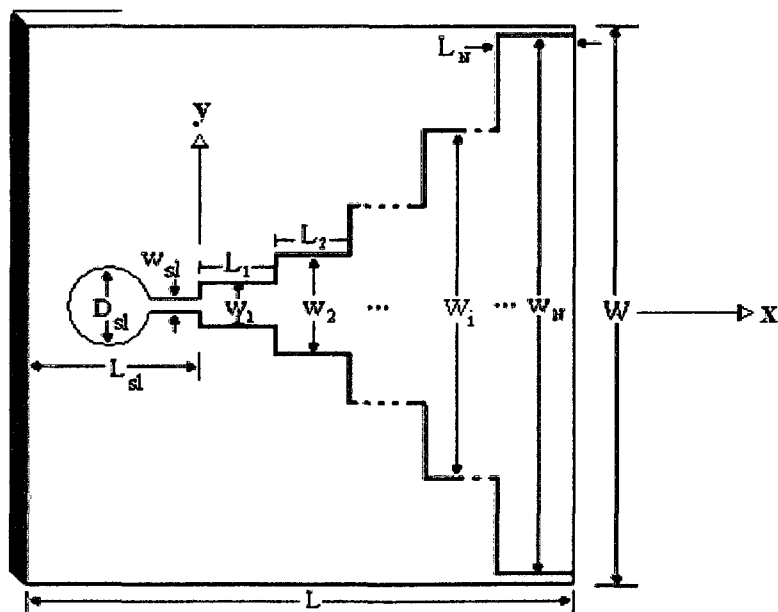


Fig. 4-2 Tapered Slot Antenna Modeled As a Series of Steps

From the x_n and x_0 , one calculates

$$\varphi_n = -2 \cos^{-1} \left(\frac{x_n}{x_0} \right) \quad (4-6)$$

and

$$\omega_n = \exp(j\varphi_n) \quad (4-7)$$

The ω_n are then used to form a polynomial equation in the variable ω :

$$\sum_{n=0}^N \Gamma_n \omega^n = \Gamma_N \prod_{i=1}^N (\omega - \omega_n) \quad (4-8)$$

where the Γ_n are reflection coefficients. By matching like powers of ω these coefficients can be determined; each of them represents the reflection coefficient at one step in the transformer. Finally, the characteristic impedances for the steps are found recursively using

$$Z_{i+1} = \frac{1 + \Gamma_i}{1 - \Gamma_i} Z_i \quad (4-9)$$

The width w_i at each step is chosen to obtain the characteristic impedance Z_i , using empirical formulas such as those found in [24].

4.4 Smoothing

The effect of curvature was studied by Lee *at al.* [18] and their experience showed the taper profile and curvature both have significant impacts on the gain, and band width. Curvature radius reduction leads to an increase in the half power beam width increase. To get a smooth taper, three types of curve fits were evaluated: (1) exponential, (2) Gaussian, and (3) cubic spline. Curve fits to the top, middle, and bottom points were evaluated as well as curve fits to the combined data.

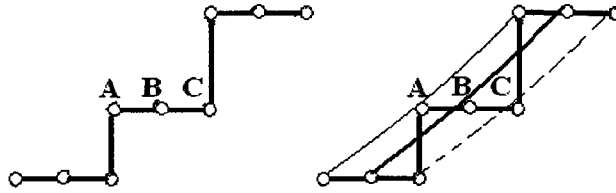


Fig. 4-3 Points Used in Curve Fit Procedure

The exponential taper has been used in many previous designs in the literature and the method presented here can be considered as a means to select a taper given a desired center frequency and overall size. The explicit formula for the curve is

$$y = a_1 e^{Rx} + a_2 \quad (4-10)$$

The Gaussian taper is

$$y = a_1 \exp\left(-\left(\frac{x - a_2}{a_3}\right)^2\right) \quad (4-11)$$

The cubic spline is defined as

$$y = a_1 x^3 + a_2 x^2 + a_3 x + a_4 \quad (4-12)$$

In the exponential and Gaussian cases, the parameters are constant for the entire curve; for the cubic spline they are defined for either of the N segments to obtain a continuous curve exactly matching the desired points.

4.5 Experimental Results

4.5.1 Dimensions and Design Parameters

For the examples here, the target size was $L = 28\text{cm}$ and $W = 17\text{cm}$, with a center frequency $f_0 = 2.0\text{ GHz}$. All designs were made on a Rogers 3206 substrate with $\epsilon_r = 6.15$ and thickness $h = 1.27\text{mm}$. The characteristic impedance of the first section was chosen as $Z_0 = 84.1\Omega$, corresponding to a slot of width $w_{SL} = 0.5\text{mm}$. The selection is somewhat arbitrary and in this case was made in order to have a low value of Z_0 for ease of transition to the micro-strip input section while still being wide enough for accurate fabrication using standard PCB processes. For the examples given here Z_L was chosen to be infinite, and $N=11$. The reflection tolerance in the transformer design was $\text{VSWR} = 2.0$ or $\Gamma_m = 0.333$. In general one can choose a finite $Z_L = k\eta_0$, but k should be chosen such that the maximum slot width w_M is more than $\lambda_0/2$ over the frequency range of interest. We found little difference in the results as long as Z_L was at least several times η_0 .

The input matching transition section (Fig. 4-4) was designed according to the method given in chapter 3. The 50Ω coaxial input was connected through a quarter-wave micro-strip transformer with one intermediate section to get to a final micro-strip section with characteristic impedance of 75.6Ω , which was computed so as to optimize the match to the initial slot-line impedance. The far side of the transition was terminated with a radial stub.

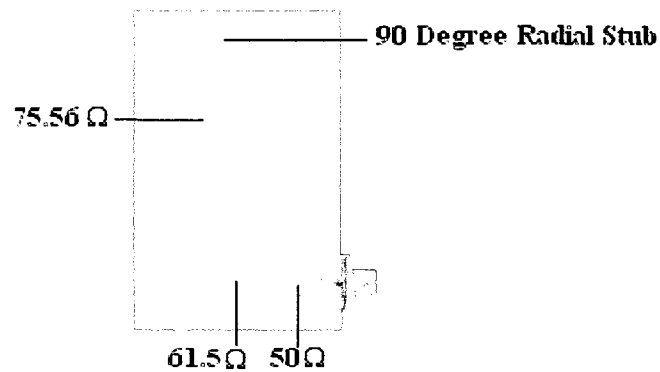


Fig. 4-4 Photograph of Micro-strip Input Matching Circuit. The Slot-line Crosses Horizontally on the Back Side Just Below the Apex of the Radial Stub.

Nine different curve fits to the computed step widths were compared, as shown in Table II. The complete antennas varied slightly in appearance, but a typical example is shown in Fig. 4-5.

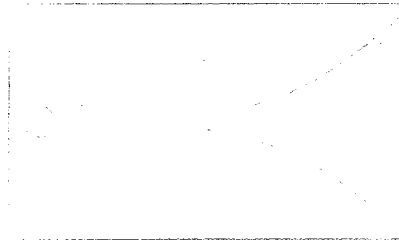


Fig. 4-5 Vivaldi Antenna the Example Shown is a Gaussian Fit to a Stepped Design

Table II - Comparison of Taper Designs with Experimental Results

In all cases the curve parameters are for dimensions in centimeters (cm).

Curve Type	Curve Parameters	Impedance Bandwidth (GHz)	Gain Bandwidth (GHz)
(1) Exponential - All points	$a_1 = 0.1372$ $a_2 = -0.1$	0.484-2.99	1.23 (1.57-2.8)

	R = 0.1546		
(2) Gaussian - All points	$a_1 = 15.41$ $a_2 = 35.34$ $a_3 = 12.15$	0.318-2.37	0.64 (1.54-2.16)
(3) Exponential - Midpoints (B)	$a_1 = 0.086$ $a_2 = -0.061$ R = 0.176	0.699-3.12	1.27 (1.58-2.85)
(4) Exponential - Top points (A)	$a_1 = 0.13$ $a_2 = -0.1$ R = 0.167	1.01-3.01	1.14 (1.66-2.8)
(5) Gaussian-Midpoints (B)	$a_1 = 14.14$ $a_2 = 34.94$ $a_3 = 13.4$	0.785-3.61	1.22 (1.68-2.9)
(6) Gaussian-Top Points (A)	$a_1 = 14.05$ $a_2 = 34.86$ $a_3 = 12.1$	0.756-3.06	1.23 (1.64-2.87)
(7) Cubic Spline-Bottom (C)	Exact fit to bottom points	0.608-3.08	1.41 (1.59-3)
(8) Cubic Spline- Midpoints (B)	Exact fit to midpoints	0.440-3.61	1.38 (1.62-3)
(9) Cubic Spline-Top Points (A)	Exact fit to top points	0.440-3.56	1.24 (1.56-2.8)

4.5.2 Impedance Bandwidth

VSWR plots for the various tapers are given in Fig. 4-6 to Fig.4-9. With the exception of the Gaussian fit to all points, all designs yield results qualitatively similar to that expected for a Chebychev transformer; however, the cubic spline fit to the midpoints has the best performance, with a bandwidth in excess of three octaves (8.2:1). This is not unexpected since this curve has the best fidelity to the idealized stepped design. It should be noted that an ultimate limit to the achievable bandwidth for all designs is set by the micro-strip transition including the radial stub. The pass-band for the Gaussian all points has a good relative bandwidth (7.45:1), but is shifted significantly lower than the others. This is a poor match to the intended center frequency of 2.0 GHz, but the lower cutoff frequency may be of interest for compact designs.

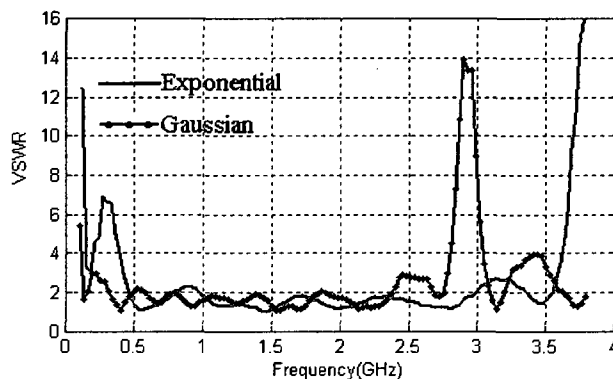


Fig. 4-6 Measured VSWR for Exponential and Gaussian All-Points Curves

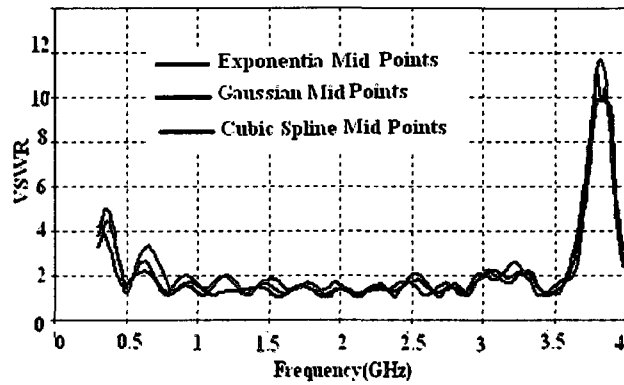


Fig. 4-7 Measured VSWR for Exponential, Gaussian, and Cubic Spline fits to Midpoints

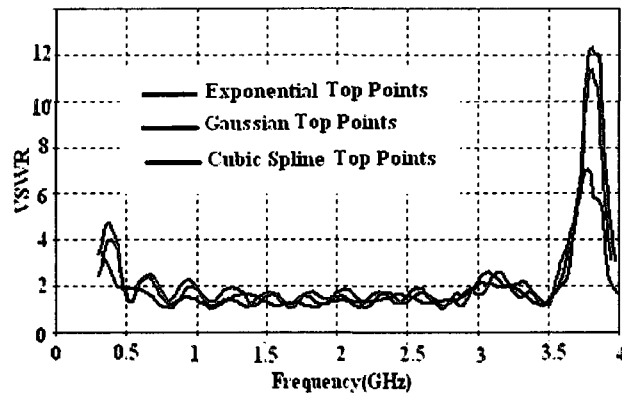


Fig. 4-8 Measured VSWR for Exponential, Gaussian, and Cubic Spline Fits to Top Points

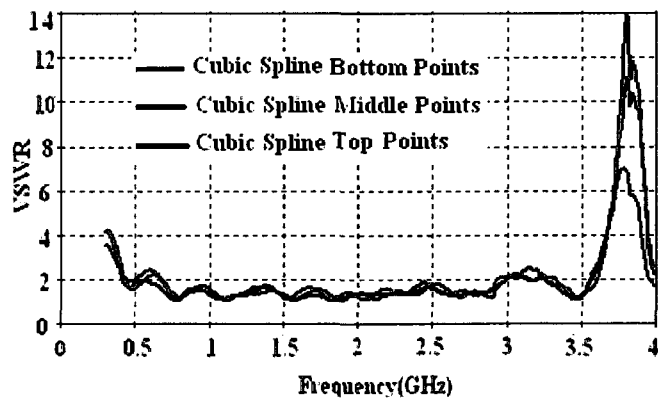


Fig. 4-9 Measured VSWR for Three Different Cubic Spline Fits

4.5.3 Radiation Patterns

E- and H-plane co-polarized and cross-polarization patterns for each design at 1, 1.5, 2, 2.5, and 3 GHz are shown in Fig. 4-10 to Fig. 4-19. All designs show patterns typical of Vivaldi type antennas, with peak gain on bore-sight of 10 +/- 1 dBi at the design center frequency, and front-back ratios of at least 10 dB and typically >15 dB.

Bore-sight gain versus frequency is compared in Fig. 4-19. The best uniformity across the center of the pass-band is obtained with a Gaussian taper; however, the best gain bandwidth measured at the 3 dB points relative to the peak is obtained for the cubic spline tapers.

Cross-polarized patterns were also taken for all nine designs. A single example typical of all the cases is shown in Fig 4-19. In general the cross-polarization was down >20 dB compared to the peak gain in both planes.

For gain band width the gain versus frequency for designs are given in Fig. 4-20. And Fig. 4-21 shows the experimental fabrications.

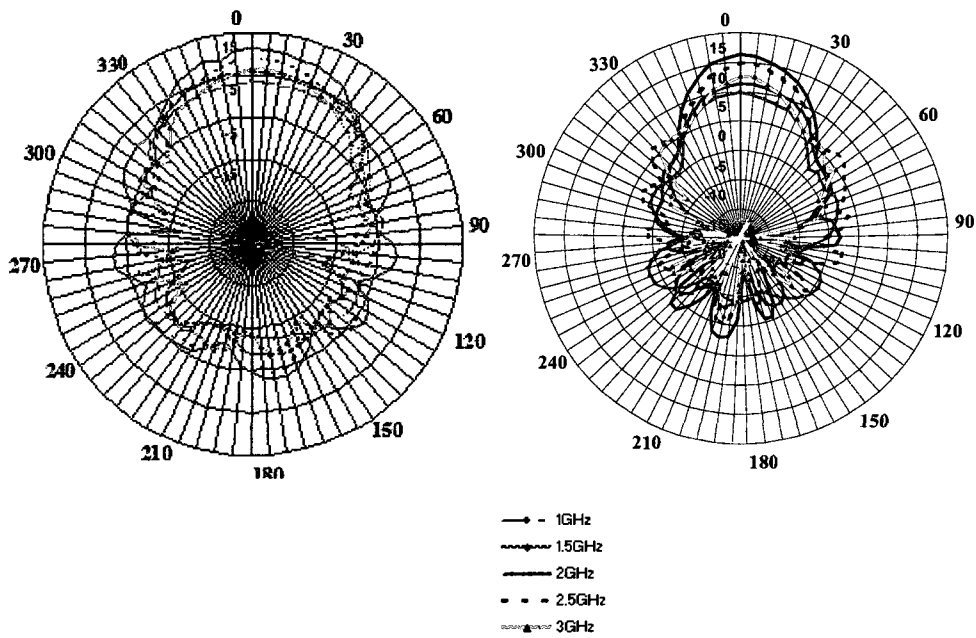


Fig. 4-10 Radiation Pattern, Exponential All Points Curve (Design #1)

Left: H-plane, Right: E-plane

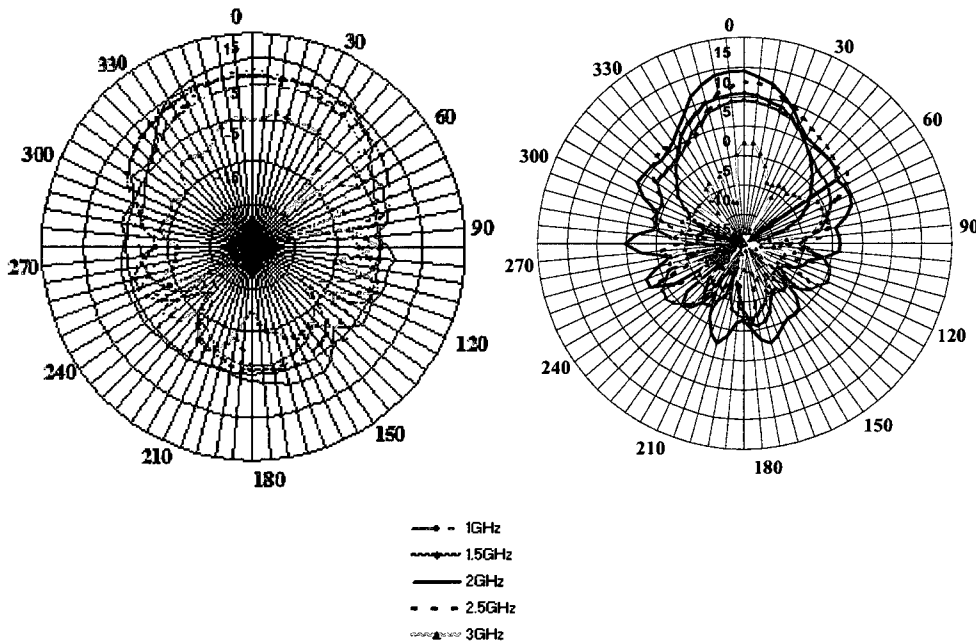


Fig. 4-11 Radiation Pattern, Gaussian All Points Curve (Design #2)

Left: H-plane, Right: E-plane

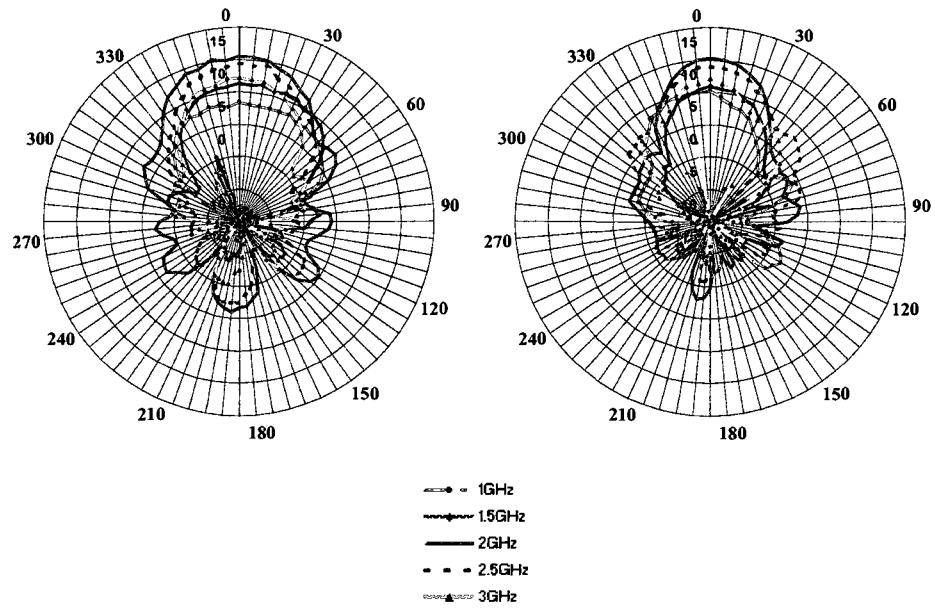


Fig. 4-12 Radiation Pattern, Exponential Midpoints Curve (Design #3)

Left: H-plane, Right: E-plane

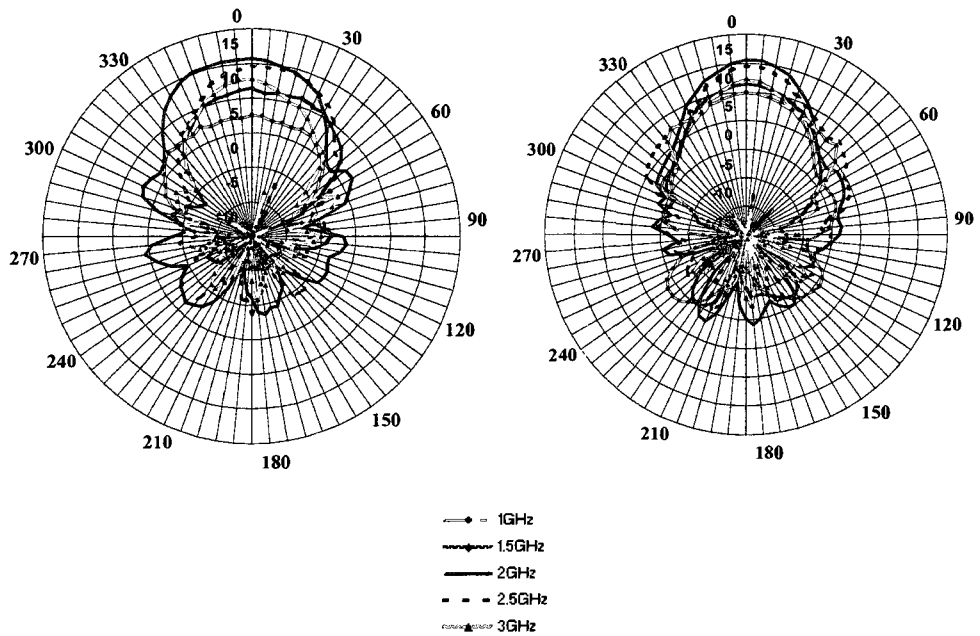


Fig. 4-13 Radiation Pattern, Exponential Top Points Curve (Design #4)

Left: H-plane, Right: E-plane.

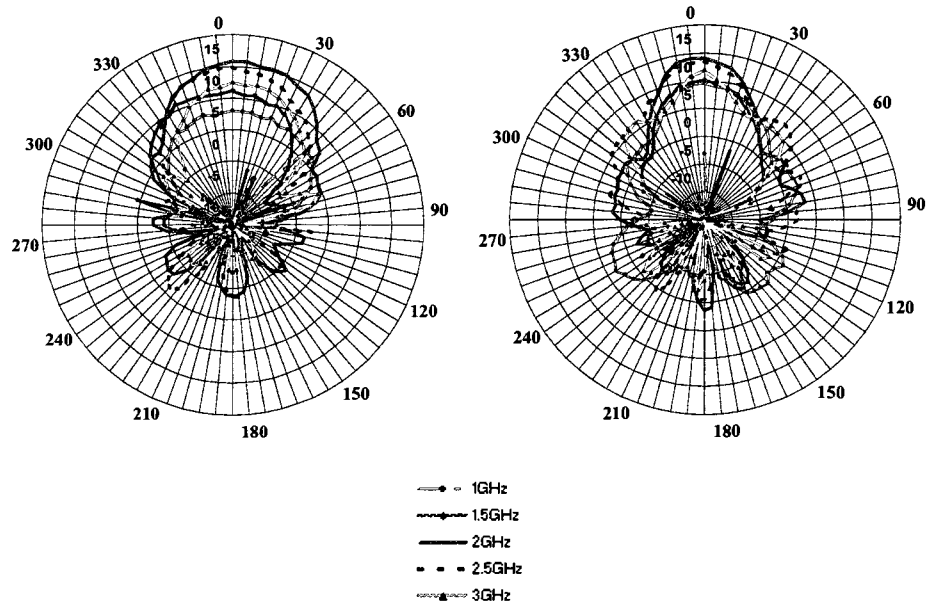


Fig. 4-14 Radiation Pattern, Gaussian Midpoints Curve (Design #5)

Left: H-plane, Right: E-plane

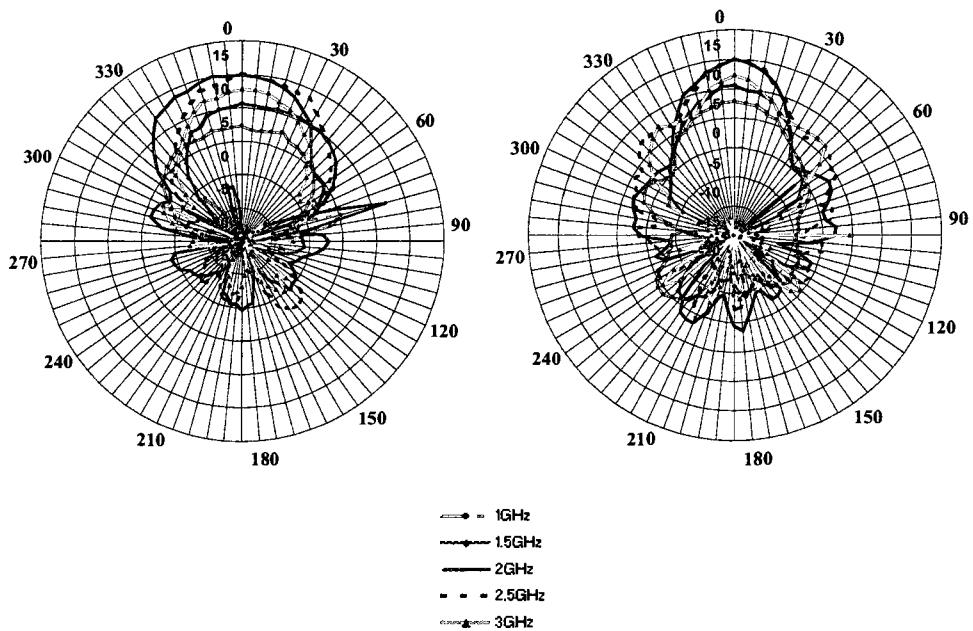


Fig. 4-15 Radiation Pattern, Gaussian Top Points Curve (Design #6)

Left: H-plane, Right: E-plane

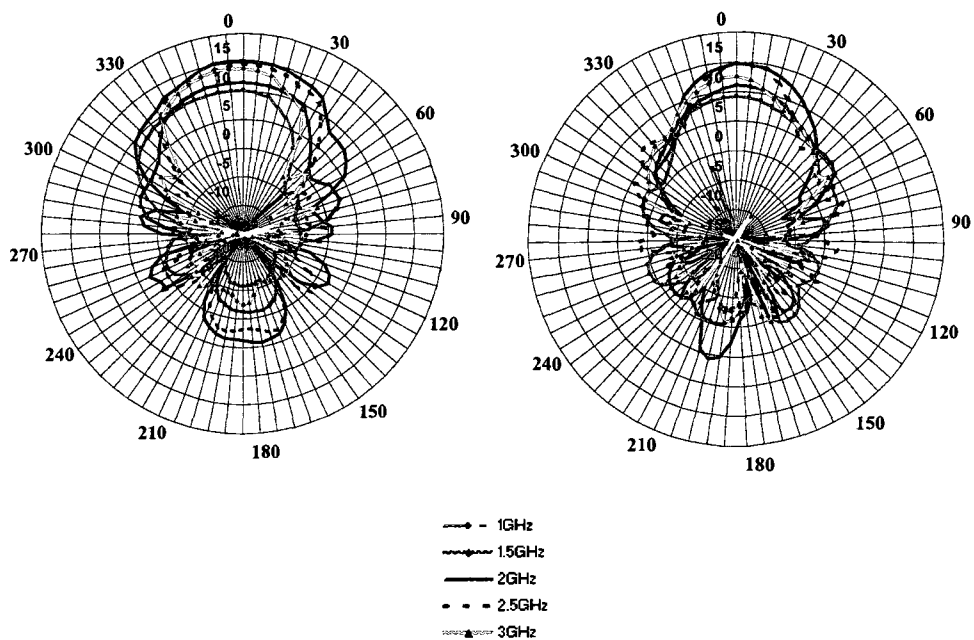


Fig. 4-16 Radiation Pattern, Cubic Spline fit to Bottom Points (Design #7)

Left: H-plane, Right: E-plane

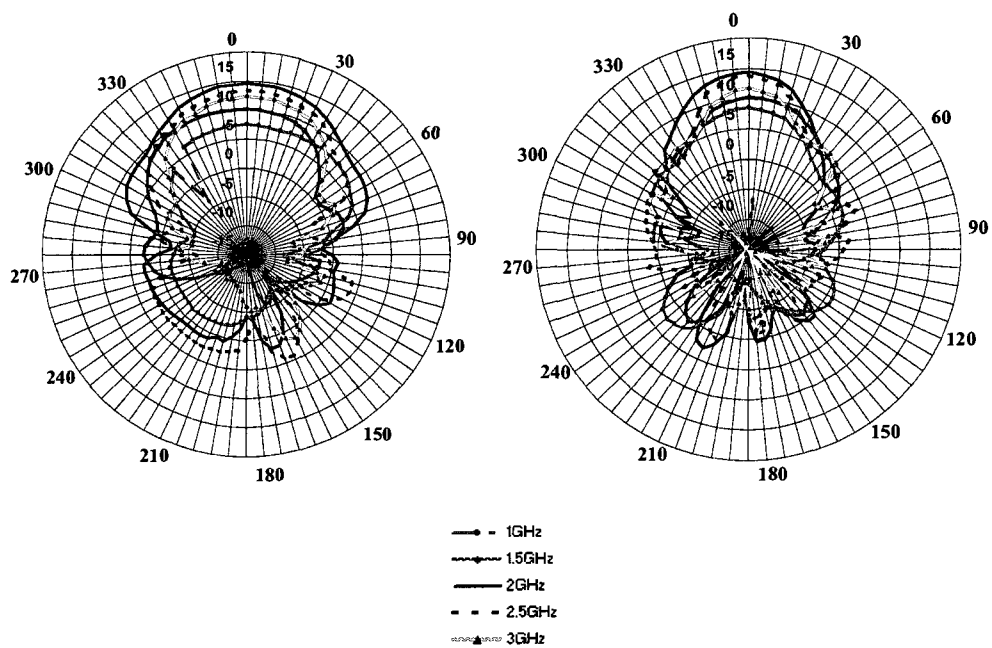


Fig. 4-17 Radiation Pattern, Cubic Spline fit to Midpoints (Design #8)

Left: H-plane, Right: E-plane

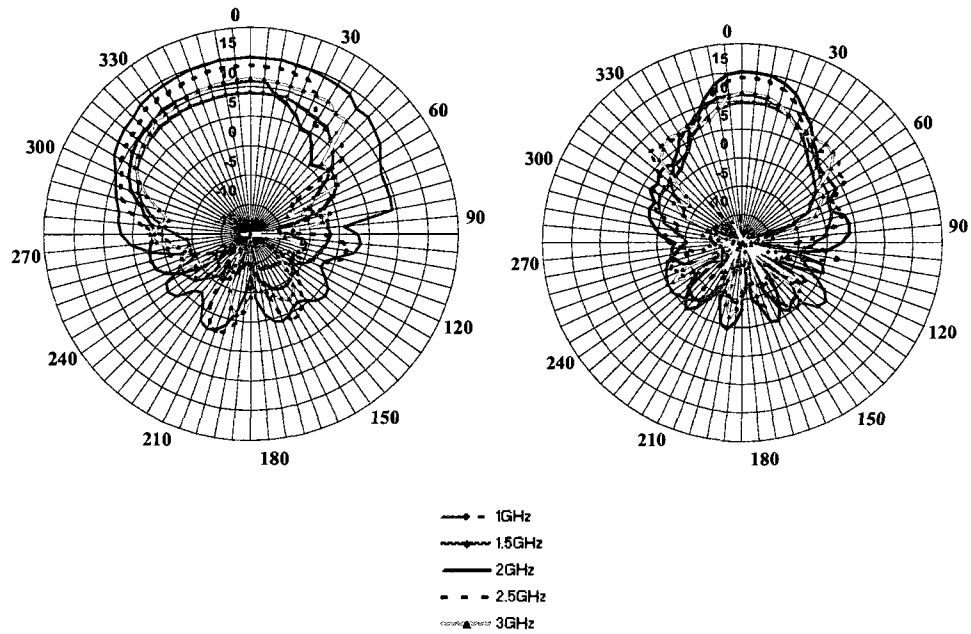


Fig. 4-18 Radiation Pattern, Cubic Spline fit to Top Points (Design #9)

Left: H-plane, Right: E-plane

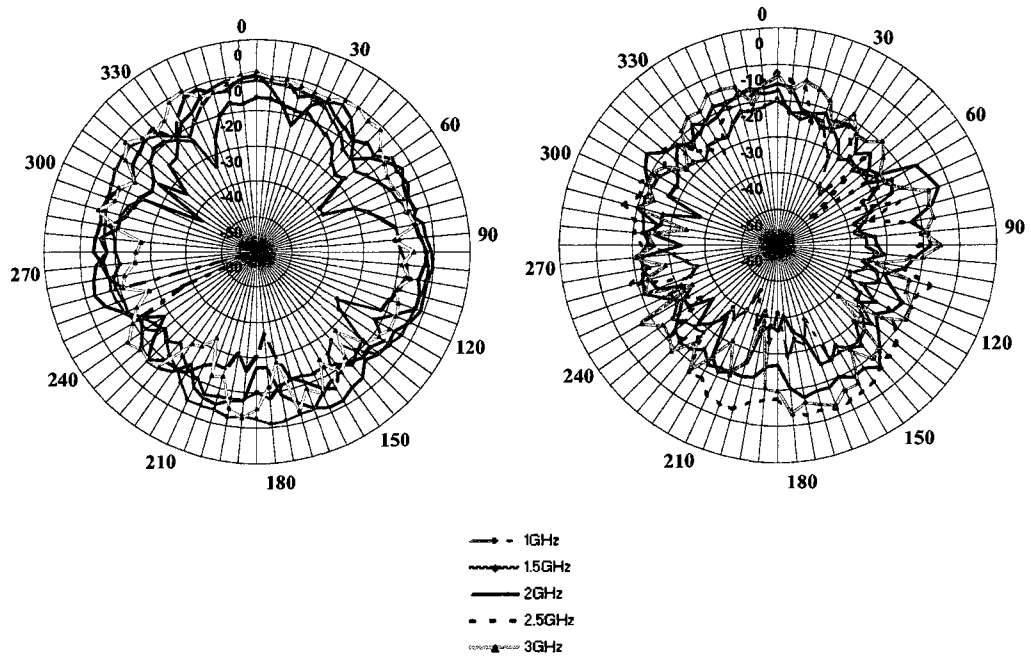
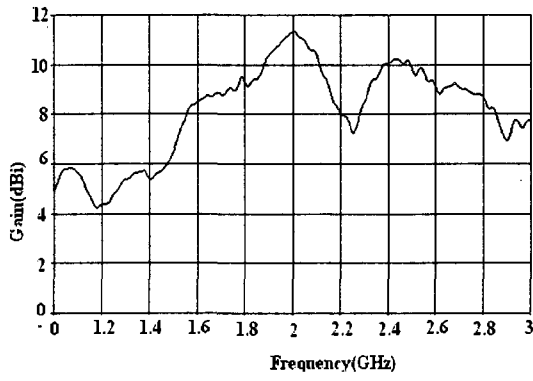
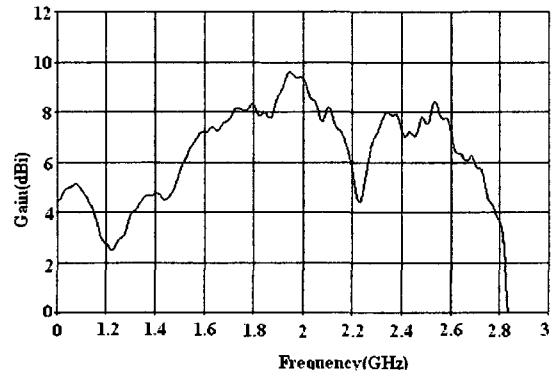


Fig. 4-19 Example Cross-Polarization Patterns

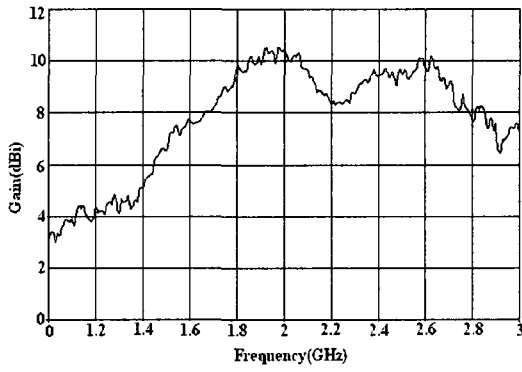
Gaussian Midpoints (Design #5) Left: H-plane, Right: E-plane.



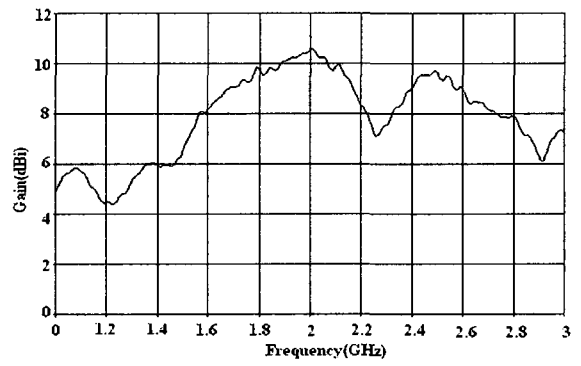
(a)



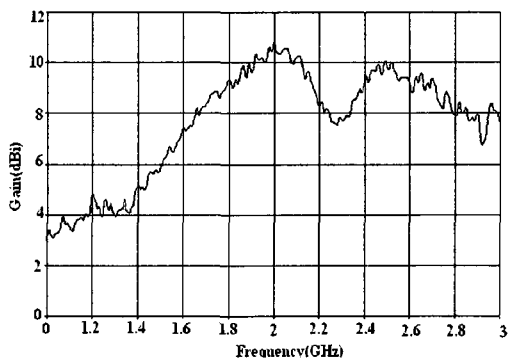
(b)



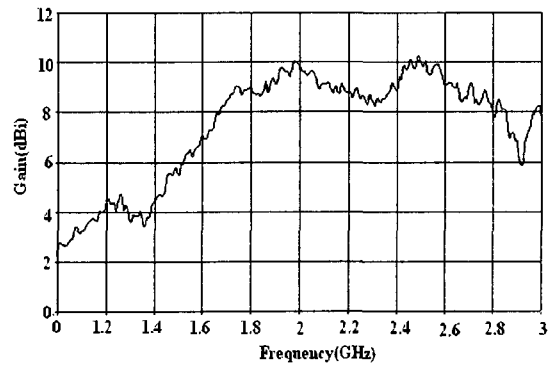
(c)



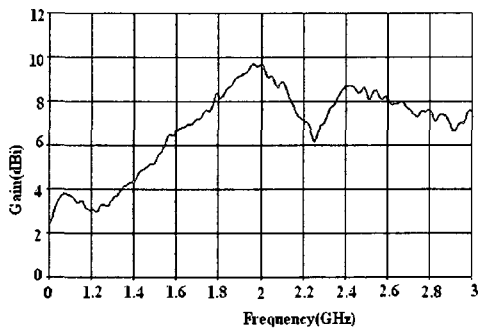
(d)



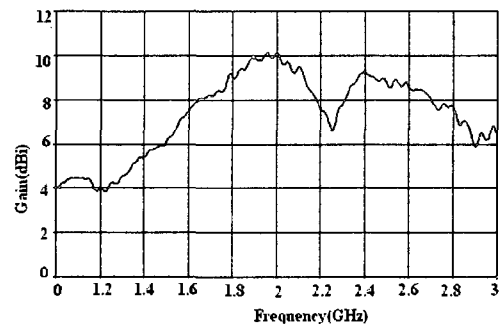
(e)



(f)

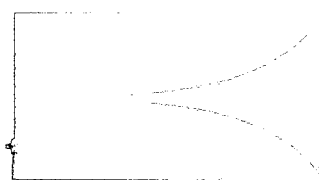


(g)

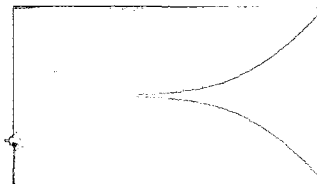


(h)

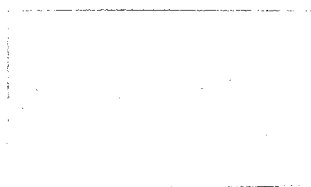
Fig .4-20 Gain vs frequency for the different taper fits: (a) Exponential all points, (b) Gaussian all points, (c) Exponential midpoints,(d) Exponential top points, (e) Gaussian midpoints, (f) Gaussian top points, (g) Cubic Spline bottom points, (h) Cubic Spline midpoints,and (i) Cubic Spline top points



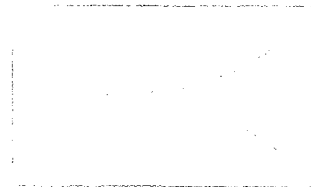
Overall-Exponential



Overall-Gaussian



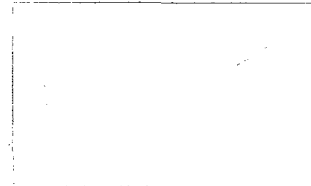
Exponential-Middle Points



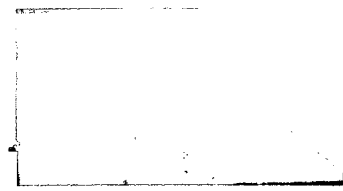
Gaussian-Middle Points



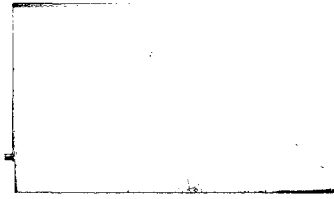
Exponential Top Points



Gaussian Top Points



Cubic Spline-Bottom



Cubic Spline-Mid



Cubic Spline-Top

Fig. 4-21 Experimental Fabricated for Different Taper Fit Over The Calculated Steps

4.6 Conclusions

The proposed method for the design of Vivaldi antenna tapers, while not perfectly optimum, provides designs with good bandwidth performance with relatively low computational requirements. Three types of curve fit to the calculated steps by this method were implemented and compared in terms of VSWR and gain bandwidth. It was found that a cubic spline curve fit to the midpoints of the stepped design simultaneously provides a broad VSWR pass-band symmetric about the center frequency combined with gain bandwidth greater than that of exponential and Gaussian curves.

CHAPTER 5

VIVALDI ANTENNA TAPER DESIGN TO PENETRATE TISSUE-Like OBJECTS

An alternative non-invasive method to X-rays in industrial and medical applications, which was proposed in early 1980s, was microwave imaging of the dielectric constant profile. The main benefit of microwave imaging is its low energy in comparison with ionizing methods, which leads to improved safety. In this paper we introduce a new and simple method based on impedance matching to reduce the effects of reflection at the object surface and increase penetration of EM waves, especially in the lower frequency range below 3 GHz.

The Vivaldi antenna, which is a Tapered Slot Antenna (TSA) with directional end-fire radiation, is the basis of the design. It includes a tapered slot-line fabricated on one side of a non-conducting substrate and a micro-strip feed/transition structure on the other side. The impedance and gain bandwidth are determined by a number of factors, including among others, the slot taper. In previous work the impact of the taper profile on gain and impedance bandwidth was studied and it was shown a cubic spline taper fit to steps approximating a Chebyshev transformer has favorable performance. In this chapter the method in [25] is extended and applied to matching to some material structure, specifically materials similar to human tissue.

5.1 Impedance Calculation

An analytical method was presented for a double layer slot-line including sandwich form and composite substrate and a closed-form expression was obtained for effective permittivity, characteristic impedance, and signal wavelength in those structures.

Here, the method of [25] is extended to the general case of a slot-line with multiple material layers. After conformal mapping the entire structure appears as shown in Fig.5-3.

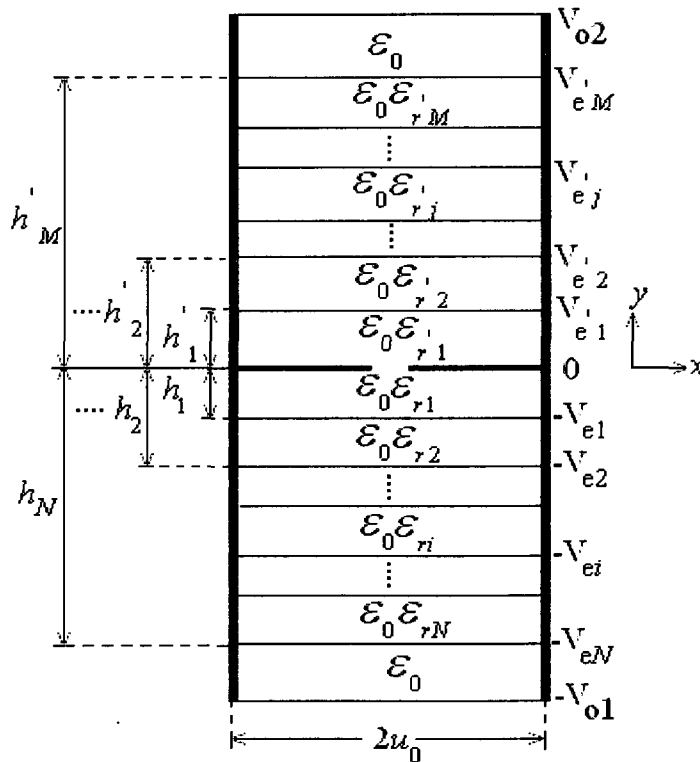


Fig.5-1 Final Conformal Mapping of Whole Layers of Slot-Line

Closed formulas for ϵ_{eff} and Z_0 , the characteristic impedance is given in the following

steps:

$$C = \epsilon_{eff} C_0 \quad (5-1)$$

where C is the capacitance with and C_0 without a dielectrics where as shown in Fig.5-3:

$$C_0 = \epsilon_0 \frac{V_{01} + V_{02}}{2u_0} \quad (5-2)$$

and,
$$C = \sum_{i=1}^N C_i + \sum_{j=1}^M C_j + C_{air(N)} + C_{air(M)} \quad (5-3)$$

Such that:

$$C_i = \epsilon_0 \epsilon_{ri} \frac{V_{ei} - V_{e(i-1)}}{2u_0}; \text{ where } V_{e0} = 0 \quad (5-4)$$

$$C_j = \epsilon_0 \epsilon_{rj} \frac{V_{e0} - V_{e(j-1)}}{2u_0}; \text{ where } V_{e'0} = 0 \quad (5-5)$$

$$C_{air(N)} = \epsilon_0 \frac{V_{01} - V_{eN}}{2u_0}, \text{ and } C_{air(M)} = \epsilon_0 \frac{V_{02} - V_{e'M}}{2u_0} \quad (5-6)$$

The dimensions in Fig.5-3 are given by (5-7) and (5-8):

$$\frac{u_0}{V_{0k}} = \frac{1}{2} \frac{K(k_{0k})}{K(k'_{0k})}; k = 1, 2, \dots \quad (5-7)$$

$$\frac{u_e}{u_0} = 1 \text{ and } \frac{V_{el}}{u_e} = 2 \frac{K(k'_{el})}{K(k_{el})} \quad (5-8)$$

Where the K function is a complete elliptic integral of the first kind where calculation involving the modulus and its complement are given in (5-9)-(5-13). By replacing each in (5-1) one can have:

$$\begin{aligned}
\varepsilon_{eff} = & 1 + [(\varepsilon_{rN} - 1) \frac{K(k'_{\varepsilon N})}{K(k_{\varepsilon N})} + (\varepsilon_{r(N-1)} - \varepsilon_{rN}) \frac{K(k'_{\varepsilon(N-1)})}{K(k_{\varepsilon(N-1)})} + \\
& \dots + (\varepsilon_{r1} - \varepsilon_{r2}) \frac{K(k'_{\varepsilon 1})}{K(k_{\varepsilon 1})} + \\
& (\varepsilon_{rM} - 1) \frac{K(k'_{\varepsilon M})}{K(k_{\varepsilon M})} + (\varepsilon_{r(M-1)} - \varepsilon_{rM}) \frac{K(k'_{\varepsilon(M-1)})}{K(k_{\varepsilon(M-1)})} + \\
& \dots + (\varepsilon_{r1} - \varepsilon_{r2}) \frac{K(k'_{\varepsilon 1})}{K(k_{\varepsilon 1})}] \times [\frac{K(k'_{01})}{K(k_{01})} + \frac{K(k'_{02})}{K(k_{02})}]^{-1}
\end{aligned} \tag{5-9}$$

$$k_{\varepsilon r}^2 = 2 \frac{\alpha_r}{1 + \alpha_r}; \text{ where } \alpha_r = \operatorname{tgh}\left(\frac{\pi w}{2h_r}\right) \text{ for } r = 1, 2, \dots \tag{5-10}$$

$$\text{and } k'_{\varepsilon r}{}^2 = 1 - k_{\varepsilon r}^2.$$

$$k_{\varepsilon r}^2 = 2 \frac{\alpha'_r}{1 + \alpha'_r}; \alpha'_r = \operatorname{tgh}\left(\frac{\pi w}{2h_r}\right) \text{ for } r = 1, 2, \dots \text{ and} \tag{5-11}$$

$$k'_{\varepsilon r}{}^2 = 1 - k_{\varepsilon r}^2$$

$$k_{01}^2 = 2 \frac{\alpha_{01}}{1 + \alpha_{01}}; \alpha_{01} = \operatorname{tgh}\left(\frac{\pi w}{2h_{01}}\right) \text{ and } k'_{01}{}^2 = 1 - k_{01}^2 \tag{5-12}$$

$$k_{02}^2 = 2 \frac{\alpha_{02}}{1 + \alpha_{02}}; \alpha_{02} = \operatorname{tgh}\left(\frac{\pi w}{2h_{02}}\right) \text{ and} \tag{5-13}$$

$$k'_{02}{}^2 = 1 - k_{02}^2$$

The virtual distances are given below in (5-14) and (5-15)

$$h_{01} = h_N \left[1 + \frac{0.0133}{\varepsilon_{rN} + (\varepsilon_{r(N-1)} - \varepsilon_{rN}) \frac{h_{N-1} - h_{N-2}}{h_N} + \dots + (\varepsilon_{r1} - \varepsilon_{rN}) \frac{h_1}{h_N} + 2} \left(\frac{\lambda_0}{h_N}\right)^2 \right] \tag{5-14}$$

$$h_{02} = h'_M \left[1 + \frac{0.0133}{\varepsilon_{rM} + (\varepsilon_{r(M-1)} - \varepsilon_{rM}) \frac{h'_{M-1} - h'_{M-2}}{h'_M} + \dots + (\varepsilon_{r1} - \varepsilon_{rM}) \frac{h'_1}{h'_M} + 2} \left(\frac{\lambda_0}{h'_M} \right)^2 \right] \quad (5-15)$$

$$\begin{aligned} Z_0 &= \frac{\eta_0}{\sqrt{\varepsilon_{eff}}} \frac{2u_0}{V_{01} + V_{02}} \\ &= \frac{\eta_0}{\sqrt{\varepsilon_{eff}}} \left[\frac{K(k'_{01})}{K(k_{01})} + \frac{K(k'_{02})}{K(k_{02})} \right]^{-1} \end{aligned} \quad (5-16)$$

where η_0 , is free space characteristic impedance and equals to 120π .

5.2 Smoothing

After calculating the slot widths required at each step, a curve fit is used to produce a smooth taper. In previous work, Gaussian, exponential, and polynomial curves were compared. It was found that a piecewise cubic spline ($y = a_1x^3 + a_2x^2 + a_3x + a_4$) fit provides a better VSWR pass-band which is symmetric about the center frequency.

This taper form is used here.

5.3 Experimental Results

A symmetric structure (Fig.5-5) is selected. The antenna was implemented on FR-4 board with $\varepsilon_r = 4.23$ with center frequency 2.0 GHz, $H1=1.57$ mm thickness and overall size of $L=30.95$ cm by $W=7.8$ cm. An identical top layer of FR-4 board ($H1=H2$), with length equal to 27.2cm covers the slot-line to have symmetric structure. Optional water containing layers separated by polycarbonate sheets ($\varepsilon_r=1.95$) of 0.762mm thickness are filled by water ($\varepsilon_r = 77.6+j7.53$ at 2.0 GHz) and $H4=3$ mm. To lessen the water loss, an air gap was considered with $H3=1$ mm.

The characteristic impedance of the initial step was set at 52Ω , corresponding to a slot width of 1mm. The load impedance was chosen to be infinite and $N=22$. In general one can choose a finite $Z_L = k\eta_0$, but for free space application k should be chosen such that the maximum slot width is more than $\lambda/2$ in the target material over the frequency range of interest. The fabricated antenna beside a quarter coin is shown in Fig.5-6.

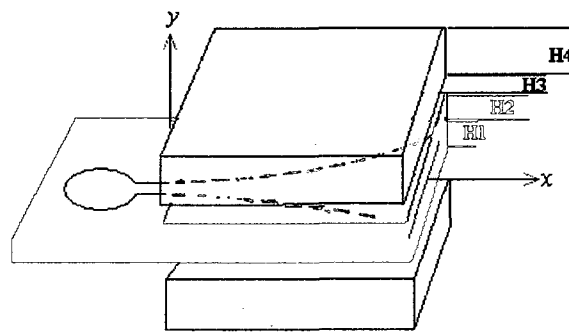


Fig.5-2 Selected Structure for Empirical Verification



Fig.5-3 Antenna Practical Example

For an initial comparison, we measured input reflection coefficient for a commercial 1-18 GHz double ridged horn, single layer Vivaldi antenna, and two multilayer Vivaldi antennas. One of the multilayer antennas had FR-4, air and water layers on each side as described above, the other was a simple FR-4 sandwich. In all cases the mouth of the antenna was pressed against a thin-walled container of water.

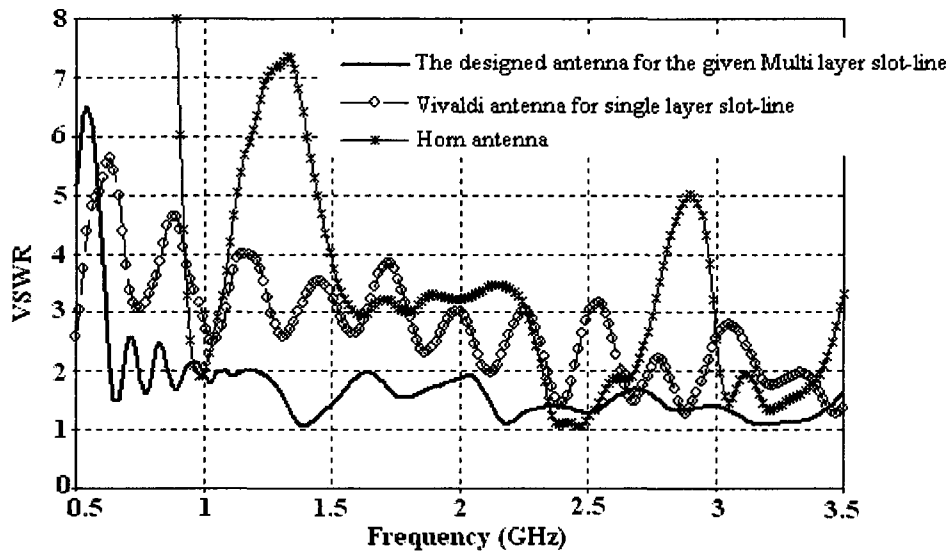


Fig.5-4 VSWR Results

Fig. 5-7 compares the VSWR for the horn, the single layer slotline, and the slotline with air and water layers. The multilayer structure has lower reflection over the entire frequency range and is significantly better at low frequency. This could be especially useful in reducing clutter in reflection-based imaging systems. However, part of the improved VSWR performance is undoubtedly due to absorption in the water layers.

As a second comparison, transmission through a 60cm tank of water was measured with using the horn, the single layer Vivaldi, and the FR-4 sandwich Vivaldi as transmit antennas, with a horn as the receive antenna. While all three have comparable performance, the horn has slightly better performance.

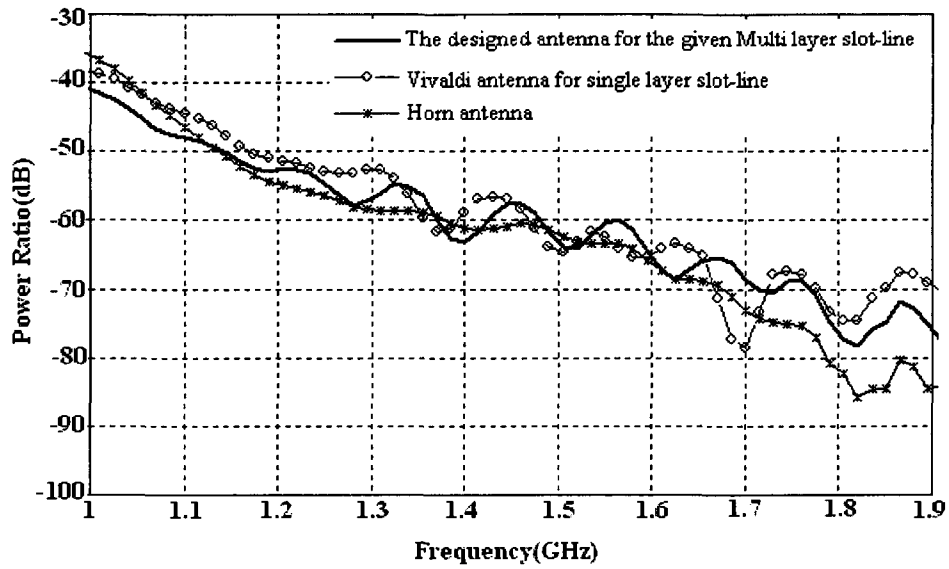


Fig.5-5 Transmission Results

CHAPTER 6

UWB PERFORMANCE OF VIVALDI ANTENNAS

In this chapter a set of Vivaldi antennas are quantitatively compared using a number of time domain figures of merit. The antennas are first characterized in the frequency domain using calibrated scattering parameter measurements including de-embedding. The time domain responses are then computed from the frequency domain scattering parameter data using digital signal processing techniques. Finally the time domain data is processed to determine the descriptors with which the antennas are evaluated and compared.

6.1 Introduction

The performance of an UWB antenna can often be most advantageously described with quantities or descriptors natural to the time domain including, for example, energy gain, rise time, and impulse response width. Of course it is natural to compute such quantities from time domain data resulting from a fast rise-time source signal and measured directly with a high-speed digital sampling oscilloscope. However, because the physical system comprised by an antenna and the surrounding space behaves as a linear time invariant (LTI) system, it is possible to bring to bear many highly-refined tools such as the FFT as well as advanced windowing techniques to effectively transform data measured in the frequency domain into accurate time domain data. Frequency domain measurements, in turn, exploit the sophisticated calibration and de-embedding procedures developed for automatic vector network analyzers. Moreover, the use of phase sensitive detection in such measurements typically provides superior signal to noise ratio. The remainder of this chapter is organized into the following sections which includes a general exposition of the design of the Vivaldi antennas. It comprises four subsections including (1) a general approach for the synthesis of the requisite impedance tapers, (2) an approach for realizing the impedance tapers in a multilayer slot-line, (3) the details of the specific slot line tapers employed in this work, and (4) a discussion of the micro-strip to slot-line transitions. After that the measurement method, which is based on a complex frequency-domain three-antenna approach, is described in some detail. The measured frequency domain data is presented along with some discussion of the frequency domain characteristics. And the transformed time domain data in the form of the impulse response is presented. Also, the subsequent data reduction to time domain antenna

descriptors is addressed. The energy gain and rise time of the transitions is presented. Finally, some general conclusions concerning the utility of the three tapers are drawn.

6.2 Feed Structure

The feed structure is a crucial component of the Vivaldi antenna and in some cases is the limiting component in terms of frequency range. The broadband feeds for the antennas presented here were described in chapter 3. The feed structure employs two cascaded quarter-wave matching sections implemented in the micro-strip line which lead to a micro-strip to slot-line crossover type transition. The cascaded quarter wave matching sections, despite their designation as quarter-wave, function in concert with a shorted stub and the open-circuit behind the taper to provide nearly three octaves of operating bandwidth. The stub on the far side is terminated with a 90 degree radial stub to provide a very broad band short circuit. It is possible to consider this transition as the dual of a Marchand balun or a Roberts dipole; that is it is topologically similar to the so-called compensated balun .

6.3 Antennas Used in This Experiment

The three antennas constructed and measured for this experiment are summarized in Table I below.

Table III. Antenna Parameters

	A1	A2	A3
Taper type	Cubic spline top points	Cubic spline midpoints	Cubic spline top points
Layers	Single layer dielectric, RO3206	Single layer Dielectric. RO3206	Sandwiched two layers, FR-4
ϵ_{r1}	6.15	6.15	4.23
ϵ_{r1}'	none (1.0)	none (1.0)	4.23
Total length	295.6mm	295.5mm	309.5mm
Total width	196mm	170mm	78mm

All of the designs have a center frequency of 2 GHz. The single layer antennas (A1 and A2) are implemented on Rogers 3206 with $\epsilon_r = 6.15$ and the multilayer (A3) on FR-4 board with $\epsilon_r = 4.23$. FR-4 in comparison with Rogers one has much more absorption, and in the high frequency response shows poor transmission, however, the FR-4 multilayer performs close to the other antennas in the range 1-2 GHz. The single layer designs have cubic-spline taper fit to middle and top points and the multilayer one has a

top points fit. In previous experiments which presented in chapter 4 the top point fit showed better results in terms of reflection and transmission.

6.4 Measurements

As presented, the designed antennas are not identical, so to measure the antennas complex transfer functions the three antenna method was used. By expanding the formula in the complex transfer function can be calculated as:

$$H_{A_1}(\omega) = \sqrt{\frac{2\pi RC}{j\omega} \frac{S_{21}^{A_3A_1}(\omega)S_{21}^{A_1A_2}(\omega)}{S_{21}^{A_2A_3}(\omega)}} e^{j\omega R/C} \quad (6-1)$$

Where A_1 , A_2 , and A_3 denote the sequence of antennas, C the speed of light, S_{21} the forward transmission coefficient for a reciprocal two-port network between antennas 1 and 2, and R the physical distance between antennas. The other complex transfer function for the other antennas can be calculated by the circular permutation of the antenna indexes in the formula. The frequency step, in the measurements should be such that $\Delta f < C/R$. The step in this case is 3.75 MHz compared to minimum criteria of 60 MHz. This condition is needed for proper unwrapping of the phase function.

6.5 Frequency Domain Data

Three antennas including two single-layer and one multilayer slot-line Vivaldi antennas were selected to analyze their impulse response. In Fig. 6-1, the magnitude of the frequency domain transfer functions of the three antennas is presented. As given, the bandwidth of all three is quite good, extending down below 500 MHz and up to nearly 4 GHz. The notch near 3800MHz appears to be due to the micro-strip to slot-line transition. Efforts are underway to develop an improved transition for the multilayer VA by using

RT-Duroid board which has less absorption than FR-4 for improved penetration and transition.

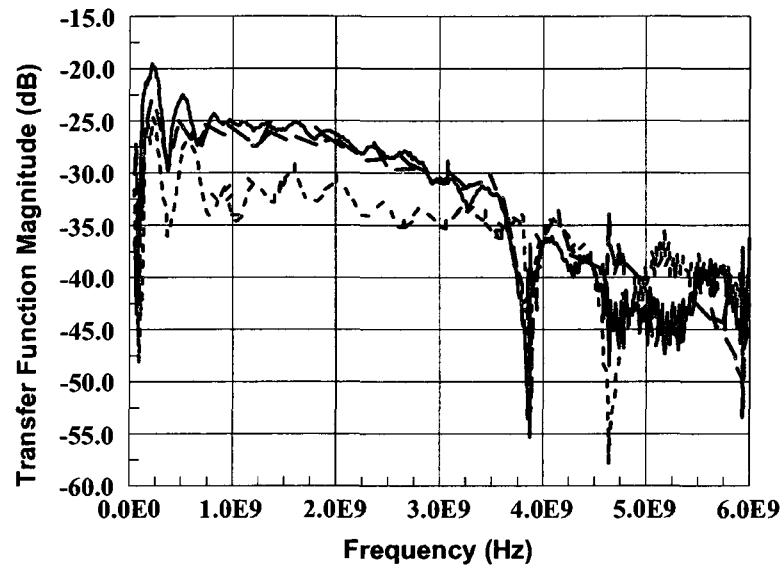


Fig. 6-1 Transfer Function Magnitude

Black solid line - A1

Green long dashes - A2

Blue short dashes - A3

6.6 Time Domain Data

The time-domain impulse responses of the three Vivaldi antennas have been computed from the complex frequency-domain transfer functions using FFT techniques, frequency-domain windowing, and extrapolation of the data. In Fig. 6-2, the three impulse responses are shown on a coarse time scale in order to include all of the significant ringing. In Fig. 6-3, the early-time impulse responses are presented on a fine time scale to show the rise time as well as the negative-going precursor. Note that as described in, the extracted distance, R , in the three-antenna approach for determining the

frequency-domain transfer functions is necessarily arbitrary. Thus, the time origin in Figs. 6-2 and 6-3 is also arbitrary. Note that the frequency of the ringing in the impulse responses is equal to that of the notch in the frequency domain transfer function data. As noted earlier, this behavior is due to the transition and not to reflections at the mouth of the antenna. In Table IV, the rise times of the impulse responses are presented. As can be seen, the rise times are all approximately 80 picoseconds. It is worth while to note that although the response of antenna A3 is smaller in magnitude than that of the other two antennas, the time response is significantly better in terms of the overall length. Moreover, this reduction in length does not come at the expense of rise time as is shown by the data in Table IV.

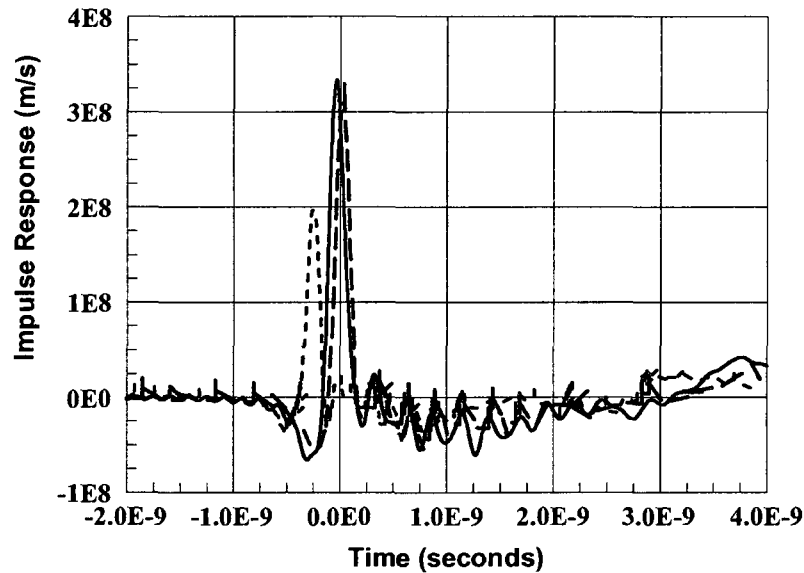


Fig. 6-2 Impulse Responses

Black solid line - A1

Green long dashes - A2

Blue short dashes - A3

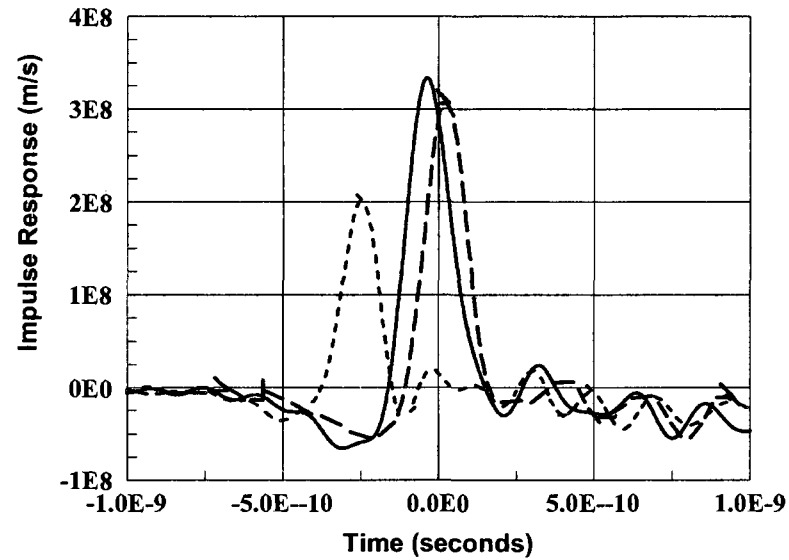


Fig. 6-3 Impulse Responses

Black solid line - A1

Green long dashes - A2

Blue short dashes - A3

Table IV. Impulse Response Parameters

Antenna	Peak (m/s)	Rise Time (ps)	Pulse Width (ps)	Max Slope (m/s²)
A1	3.34×10^8	81	264	3.7×10^{18}
A2	3.12×10^8	85	232	3.3×10^{18}
A3	2.02×10^8	82	199	3.3×10^{18}

6.7 Conclusions

In this chapter we study the impulse response of the Vivaldi antenna with a cubic spline taper incorporating two different designs one using a single layer substrate, *mostly applied mainly in communication systems*, and other being the multilayer dielectric model with greater penetration depths. Experimental results were acquired related to obtain both frequency and time domain responses. Our finding was that the cubic spline provides a good bandwidth for all designs, although the FR-4 dielectric VA has greater absorption leading to reduction of the magnitude of the transfer function.

The designs time domain or impulse response of all the designs showed that the frequency of the ringing in the impulse responses and the notch in the frequency domain transfer function data are equal. We conclude that the multilayer design provides better over all length in time domain response in comparison to single layer ones.

REFERENCES

- [1] A. Joisel, J. Mallorqui, A. Broquetas, J. M. Ge_rin, N. Joachimowicz, M. V. Iossera, L. Jofre and J. -C. Bolomey, "Microwave Imaging Techniques for Biomedical Applications," Instrumentation and Measurement Technology Conference, 1999.
- [2] Tommy Gunnarsson, "Microwave Imaging of Biological Tissues: The Current Status in the Research Area" December 18, 2006.
- [3] S. Y. Semenov, R. H. Svenson, A. E. Boulyshev, A. E. Souvorov, V. Y. Borisov, Y. Sizov, A. N. Starostin, K. R. Dezern, G. P. Tatsis and V. Y. Baranov, "Microwave Tomography: Two-Dimensional System for Biomedical Imaging," IEEE Transactions on Biomedical Engineering, Vol-43, No. 9, pp. 869–877, September 1996.
- [4] J. M. Geffrin J. J. Mallorqui, N. Joachimowicz R. Redondo, M. Vall-Iossera O. Franza, A. Joisel and J. -C. Bolomey, "Reconstruction of the Model Noise in Non-Linear Reconstruction via an Efficient Calculation of the Incident Field: Application to a 434 MHz 37 Scanner," Antennas and Propagation Society 1999 IEEE International Symposium, Vol-2, pp. 996–999, July 1999.
- [5] K. D. Paulsen, P. M. Meaney, "Nonactive Antenna Compensation for Fixed-Array Microwave Imaging—Part I: Model Development", IEEE Transactions on Medical Imaging, Vol. 18, pp. 496–507, June 1999.
- [6] J. B. Knorr, "Slot Line Transition", IEEE Transactions on Microwave Theory and Techniques, Vol.22, May 1974, pp. 548-554.
- [7] D. Chambers, S. B. Cohm, E. G. Christol, and F. Young, "Microwave Active Network Synthesis", Stanford Best Inst., Menlo Park Calif., Contract DAAB07-C-0044, SRI project 8254, June 1970.
- [8] Bernd Schuppert, "Microstrip/Slotline Transitions: Modeling and Experimental Investigation ", IEEE Transaction on Microwave Theory and Techniques, Vol. 36, No.8, August 1988, pp.1272-1282.
- [9] A. Podcameni and M. L. Coimbra, "Slotline-Microstrip Transition on iso/anisotropic Substrate: a More accurate Design," Electronics Letters, vol. 16, no. 20, pp. 780-781, 1980.

- [10] J. B. Knorr and J. Saenz, "End Effect in a Short Stub", IEEE Transaction on Microwave Theory and Techniques, MTT-21, pp.579-581, Sep. 1973.
- [11] S. B. Cohn, "Slot line on a dielectric substrate," IEEE Transaction on Microwave Theory and Techniques, Vol. MTT-17, pp. 768-778, 1969.
- [12] H.Y. Yang and N.G. Alexopoulos, "A Dynamic Model for Microstrip-Slotline Transition and related Structures", IEEE MTT-S Digest, pp. 773-775, 1987.
- [13] P. Silvester and P. Benedik, "Equivalent Capacitance of Micro-strip Open Circuit", IEEE Transactions on Microwave Theory and Techniques, Vol. MMT 20, No. 8, August 1972, pp. 511-516.
- [14] Y.H. Choung and W.C. Wong, "Microwave and Millimeter-Wave Slotline Transition design" Microwave Journal, Vol.37, No.3, pp. 77-89, 1994.
- [15] Joon Shin and Daniel H. Schaubert, " A Parameter Study of Stripline-Fed Vivaldi Notch-Antenna Arrays", IEEE Transaction on Antenna and Propagation, Vol. 47, No.5, pp.879-886, May 1999.
- [16] P.J Gibson, "The Vivaldi Aerial", Proc. 9th European Microwave Conference, 1979, pp. 101-105.
- [17] D.A. Burrell and J.T. Aberle, "Characterization of Vivaldi Antennas Utilizing a Microstrip-to-Slotline Transition", IEEE CNF, 1993, pp. 1212-1215.
- [18] Richard Q. Lee and Rainee N. Simson, "Effect of Curvature on Tapered Slot Antennas", NASA Lewis Research Center NYMA Group, pp. 188-191.
- [19] Sang-Gyn Kim and Kai Chang, "Ultra Wideband Exponentially-Tapered Antipodal Vivaldi Antennas", IEEE Antenna and Propagation International Symposium, pp. 2273-2276, 2004.
- [20] Kai Fong Lee and Wei Chen, " Advanced Microstrip and Printed Antennas", Wiley Series in Microwave and optical Engineering, 1997.
- [21] Homayoon Oraizi, Shahrokh Jam, "Optimum Design of Tapered Slot Antenna Profile", IEEE Transaction on Antenna and Propagation, Vol. 51, No. 8, August 2003.

- [22] Sreenivas Kasturi, Daniel Schaubert, "Effect of Dielectric Permittivity on Infinite Arrays of Single-Polarized Vivaldi Antenna", *IEEE Transaction on Antenna and Propagation*, Vol.54, No.2, February 2006.
- [23] Adrian T. Sutinjo and Edwin Tung "The Design of a Dual Polarized Vivaldi Array", *Microwave Journal*, September 2004.
- [24] K.C Gupta, Ramesh Garg, Inder Bahl and Prakash Bhartia, "Microstrip Lines and Slotlines", Second Edition, Artech House Publisher, 2007.
- [25] Jiri Savaicna, "Dispersion Characteristic of Multilayered Slotlines-A Simple Approach", *IEEE Transaction on Microwave Theory and Techniques*, vol. 47, No. 9, September 1999.
- [26] James S. McLean, Robert Sutton, Armando Medina, Heinrich Foltz, and Junfei Lee, "The Experimental Characterization of UWB Antennas via Frequency-Domain Measurements", *IEEE Antennas and Propagation Magazine*, pp. 192-202, 2007.
- [27] Janaswamy R., and D.H. Schaubert, "Characteristic Impedance of a Wide Slotline on Low Permittivity Substrate", *IEEE Trans. Microwave Theory Tech.*, Vol. MTT-34, pp.900-902, 1986.
- [28] George Sinclair, "The Transmission and Reception of Elliptically Polarized Waves", *Proc. IRE*, 38, February, 1950, pp. 148-151.
- [29] L. Jofre, M. S. Hawley, A. Broquetas, E. De Los Reyes, M. Ferrando and A. R. Elias-Fuste, "Medical Imaging with a Microwave Tomographic Scanner," *IEEE Transactions on Biomedical Engineering*, Vol-37, No. 3, pp. 303-311, March 1990.

BIOGRAPHICAL SKETCH

Khabat Ebnabbasi was born in Mahabad, Eastern Kurdistan (Iran) in 1979. He received the B.S. degree in electronics engineering from University of Tabriz, Iran, in 2003. He was graduated as M.Sc at University of Texas-Pan American., Texas, USA in 2009.

He developed a high speed and high resolution, sub femto Farad, capacitance measuring system for tomography and scanning applications with a specific calibration solution. He has published an electronic text book for discontinuous bachelor degree in 2006. Khabat Ebnabbasi offered a system design for medical microwave imaging which won the IEEE Microwave Theory and Techniques society (MTT-S) graduate fellowship for medical application in 2008. He won the first place in HESTEC (Hispanic Engineering, Science and technology) poster competition research symposium and was the recipient of UTPA excellence scholarship in 2008. In 2009 he was awarded Phi-Kappa-Phi honor society membership.

His research interest includes RF circuits and electronics, applied electromagnetic and Microwave.